NUMERICAL AND THEORETICAL ANALYSIS OF EXTERNAL GEAR PUMP

A Thesis

by

Deniz İmamoğlu

Submitted to the
Graduate School of Sciences and Engineering
In Partial Fulfillment of the Requirements for
the Degree of

Master of Science

in the
Department of Mechanical Engineering

Özyeğin University
January 2019

NUMERICAL AND THEORETICAL ANALYSIS OF EXTERNAL GEAR PUMP

Approved by:

Assistant Professor Dr-Ing. Özgür Ertunç,
Advisor
Department of Mechanical Engineering
Özyeğin University

Assistant Professor Dr. Altuğ Melik Başol
Department of Mechanical Engineering
Özyeğin University

Assistant Professor Dr. Bayram Çelik
Department of Astronautical Engineering
Istanbul Technical University

Date Approved: 28 January 2019

To my family and my dear friends

ABSTRACT

External gear pumps are one of the mostly used pump types in the fluid power applications due to simplicity, low cost and long operation period. However, there are some disadvantages such as internal leakages, noise and vibration with gear pumps. This study investigates comparison of theoretical calculations and 2D-3D numerical simulations with considering temperature effects on tip leakage. 2D numerical simulations have been done for pressure difference from 2 bars up to 10 bars for seven different rotational speeds. Additionally, the effect of wall temperature varied from 303 K up to 333 K has been investigated on the performance of gear pump. 3D numerical simulations could be performed only for 2 cases due to long computational time. Because of extra assumptions made in theoretical calculations for tip leakages, it is shown that there are some deviations between theoretical and numerical results. These deviations are due to pressure drop which occurs because of energy dissipation between two teeth tips which can be observed in numerical simulations and fully developed flow assumption made in theoretical analysis. Results of numerical study show that the fully developed assumption in the gap between gear tooth and wall is not appropriate. In addition, face leakage and gearing zone leakage has been investigated in 3D numerical simulations to compare with theoretical calculations. Furthermore, it has been shown that leakages increase linearly with temperature rise at the wall due to the drop in the viscosity of the liquid.

ÖZETÇE

Dıştan dişli pompalar; basit, duşuk maliyetli, uzun çalışma sureleri nedeniyle en yaygın kullanılan pompa tiplerinden biridir. Bununla birlikte, bu tip pompaların iç kaçaklar, gurultu ve titreşim gibi dezavantajları bulunmaktadr. Bu çalışmada, diş ucu kaçaklarının teorik ve 2B-3B saysal olarak karşılaştırması ve diş ucu kaçaklarına sıcaklık etkisi incelenmiştir. İki boyutlu sayısal simulasyonlar, 7 farklı donme hızında 2-10 bar arasındaki basınç farklarında yapılmıştr. Ek olarak, 303 K'den 333 K'ye kadar pompa govdesi duvar sıcaklığının dişli pompanın performansı uzerindeki etkisi araştırılmıştır.3 boyutlu sayısal simulasyonlar, uzun hesaplama suresi nedeniyle sadece iki durum için gerçekleştirilebilmiştir. Teorik hesaplamalardaki bazı varsayımlardan dolayı, sayısal simulasyonlarla arasında sapmanın olduğu gosterilmiştir. Bu sapmanın nedenleri, teorik hesaplamalardaki tam gelişmiş akış varsayımı ve sayısal hesaplamalarda iki dişli arasındaki enerji disipasyonundan dolayı oluşan basınç kaybı olduğu gosterilmiştir. Sayısal çalşmanın sonuları diş ucu ve duvar arasındaki boşlukta tam gelişmiş akış olmadığını gostermiştir. Ek olarak, 3 boyutlu sayısal simulasyonlarda teorik hesaplamalar ile karşılaştırmak için yuz kaçağı ve dişli bolgesi kaçağı araştırılmıştır. Ayrıca, duvardaki sıcaklığın artması ile birlikte diş ucu kaçağının, viskozitenin sıcaklıkla duşmesine bağlı olarak, lineer bir şekilde arttığı gorulmuştur.

ACKNOWLEDGEMENTS

I appreciate to my advisor, Dr-Ing. Özgür Ertunç for limitless support and help from the beginning to the last moment.In addition, he behaved not only as a advisor but also as a friend. Furthermore, i would like to thanks to my family for their endless support and faith and to my friends for their dear friendship.

This study was supported by the Scientific and Technological Research Council of Turkey (TUBITAK), project no:115M093. I would like to thanks them to their economical support.

TABLE OF CONTENTS

LIST OF TABLES

LIST OF FIGURES

Nomenclature

Greek and Roman Symbols

η -Dynamic viscosity

ω -Angular velocity of gear

$\otimes$ -Kronecker multiplier

ϕ -Dissipation of energy

ρ -Density

τ -Shear stress

Other Symbols

$\dot{Q}$ -Heat transfer per unit time

$\dot{W}$ -Work done per unit time

$\vec{F}_{body}$ -Body forces acting on system

$\vec{F}_{surface}$ -Surface forces acting on system

$\vec{F}_{system}$ -All forces acting on system

$\vec{n}$ -Normal vector on the control surface

$\vec{P}$ -Momentum

$\vec{U}$ -Velocity

A -Area

B -Arbitrary extensive property

b -The extensive property per unit mass

b -Tooth width

f_b -Resultant body fores acting on unit volume

h -Film thickness between tooth tip and wall

L -Top land of tooth

M -Mass

N -Number of teeth in contact with wall

P -Pressure

q -Heat flux

$Q_{t,k}$ -Mass flow rate of tip leakage

$Q_{y,k,1}$ -Mass flow rate of face leakage at first region

$Q_{y,k,1}$ -Mass flow rate of face leakage at second region

$Q_{y,k,m}$ -Mass flow rate of gearing zone leakage

r_d -Radius of gears

r_m -Radius of shaft

r_o -Average radius of gear

S_E -Energy source for unit volume

S_u -Mass source for unit volume

T -Temperature of case wall

T_v -Viscous stress tensor

U_{max} -The velocity at tooth tip

V -Volume

y -The distance away from case wall

CHAPTER I

INTRODUCTION

Gear pumps are a type of positive displacement pumps as rotates. They are used in many applications due to manufacturing simplicity, reliable operation, long life-time and relatively low production cost. They also have some disadvantages such as internal leakages, noise and vibration.

Gear pumps are classified as internal and external [2]. Internal gear pumps have an inner gear and an outer gear. Inner gear has a shaft driven by motor and its teeth are outward. Outer gear teeth are inward through the center of pump. As the inner gear rotates, it meshes with the outer gear and moves it. Fluid is trapped in gear spaces and and carried from to inlet to outlet. External gear pumps have a driving gear and a driven gear. Driving gear is driven by a motor connected to a shaft. It in turn meshes with and drives the movement of the other gear. As the gears rotate away from each other and come out mesh and they create an expanding volume on the inlet side of the pump. This creates a suction at the inlet for fluid. Then, the fluid flows into cavities and is trapped by the gear teeth as the gears rotate. A flow path is created around the outside of each one and fluid is carried through and discharged from the inlet to outlet. The contact zone between driving and driven gears, which is called gearing zone, provides sealing the moving fluid from outlet port to inlet port due to pressure difference.

External gear pumps are more robust for high pressures than internal gear pumps due to better shaft support. The maximum working pressure is approximately 250 bar for external gear pumps. Besides, this type of pumps are more compact and suitable for low/medium temperature fluids.

1.1 Literature Survey

External gear pumps are used many industries, particularly automotive in water cooling, injection and lubricating oil systems due to reliable and smooth operation for a long time [3]. However, this type pumps are prone to problems such as leakages, vibration and noise. Internal leakages affect volumetric efficiency and pump operation negatively. Three type of leakages such as face leakage, tip leakage and leakage between two gears are emphasized theoretically. Tip leakage is moving fluid through the radial clearance between tooth tip and body wall. Face leakage is the fluid amount which leaks between gears' faces and body face. Tip leakages are in safety levels when the clearance of gear tooth and the wall is between 5-15 m. But, face leakage exists at any clearances values, so the distance between wall and gear faces should be minimized with respect to production possibilities [1]. In another study, slip flow parameter is introduced to calculate the leakages based on pressure differential. The effect of slip flow coefficient on the amount of leakages for rotational speeds ranging from 250 RPM to 3500 RPM are investigated and it has been shown that slip flow coefficient reduces volumetric efficiency for constant rotational speed [4]. The floating sealing element, which is made by poly(ether-ether-ketone)(PEEK) and placed between gears' faces and body, has been developed to minimize the tip leakage and face leakage in the research. Three different designs of floating sealing elements have been tested and the best one with highest volumetric efficiency and lowest leakage have been selected based on experimental results. However, floating sealing element reduces the duration of pump due to high pressure difference (more than 35 bar) [5].

External gear pumps also can be used for low pressure applications such as fuel injection systems and Selective Catalytic Reduction(SCR) systems. Optimal design of gear pumps for exhaust gas after-treatment applications (SCR) are studied. Flow pulsations, pressure overshoots, cavitation and volumetric efficiency were optimization parameters, which have been investigated by changing the teeth number, pressure

angle and addendum-dedendum coefficient [6].

External gear pumps have moving boundaries such as driving gear and driven gear. Because of moving boundaries, numerical simulations of this type pump should be solved as unsteady. Several computational fluid dynamics studies have been done to investigate fluid flow structure inside the external gear pumps (Table 1). In the study, k- turbulence model with second-order discretization scheme for convective terms over a dynamically varying unstructured mesh has been used for rotary double external gear pump. Based on the results, reduction of clearance by 9 m, increases net flow rate by 30%. Furthermore, region at the contacting teeth near the suction side is more prone to cavitation [7]. Houzeaux and Codina [8] have simulated whole gear pump and half gear pump, which includes suction chamber and the teeth at inlet, as 2D and 3D cases. Comparison of half pump and whole pump shows that there is not much difference for pressure contours and velocity profiles. Additionally, 3D simulations give more realistic results than 2D simulations. In another research, the flow in the suction chamber of an external gear pump have been investigated. Laminar flow assumption with different turbulence models such as standard k-, realizable k-, RNG k- and Reynolds Stress Models (RSM) have been compared with each other. Based on their results, RSM turbulence model is the most suitable one according to the experimental data [9]. In another work by Castilla et al. [10], half of the gear pump using 2D and 3D simulations have been analyzied with different contact ratios. Their results show that flow rate obtained from 3D simulations are higher than that from 2D simulations with lower fluctuations in velocity magnitude both at inlet and outlet sections. In other research, CFD analysis of gear pump using with deforming mesh were studied. The simulation was modeled as unsteady, laminar and Eulerian multiphase flow. Especially, the importance of mesh deforming in the gearing zone is indicated by authors. The mesh size at deforming zone

were retained similar size with boundary cells and growth factor of mesh was minimized to improve accuracy of results. Furthermore, time step was adjusted as 0.0003 revolution per time step. External gear pump simulations have moving boundaries such as driving and driven gears. Moving boundaries makes the problem unsteady. Based on their results, coefficient of spatial variation decrease from 45% to 5.5% by increasing additive injection stream numbers at the pump intake [11]. In other work, the performance of four-stepped pump has been investigated in 3D by modeling the flow as incompressible and using finite volume method. Gear rotations have been modeled using with moving reference frame. This means there is no mesh movement or replacement in numerical simulations, but the solution have been done pretending that the gears rotates. The results of this work have been showed that experimental data and numerical simulations matched each other very well [12]. Moilan et al. have been studied dynamic behaviour of external gear pump on time dependent numerical simulations based on pressure distribution and acting torque on gears. The mesh of computational domain have been updated with data interpolation after each 1 degree rotation. The geometry of domain was half of the pump due to time consumption of numerical simulations [13].

The mesh generation in numerical simulations of external gear pumps can be performed with different methods. Overset mesh or "chimera" can be used for unsteady problems and bodies which have moving boundaries. In the study, unstructured overset mesh and mesh deformation method based on Delaunay graph mapping have been combined to generate deformable unstructured overset mesh [14]. In another study, a new method which allows time dependent anisotropic adaption for dynamic overset CFD simulations has been proposed. This method has beed used for unsteady aerodynamic interactions such as helicopter-ship and rotor-rotor interactions [15]. In the work, the performance of cycloidal rotor has been simulated with overset mesh method. The numerical simulations has been modeled as 2D and implicit unsteady

and created complex transient motions [16].

Table 1: The studies about external gear pumps numerical simulations in literature.

Authors	*Geometry*	*Mesh models*	*Flow and Turbulence Models*	*Experimental Data*
Ghazanfarian and Ghanbari, 2014 [7]	2D, all pump	Dynamic unstructured mesh	k-ϵ turbulence	Mass flow rate has been compared at different tip clearance and pressure differences
Houzeaux and Codina, 2007 [8]	2D-all pump and 3D-half pump (inlet region)	Structured at tip clearances and unstructured at the rest	Spalart-Allmaras Turbulence model	-
Castilla et al.,2010 [9]	3D- only inlet region	Deforming mesh and mesh replacement	Standard k-ϵ , realizable k-ϵ, RNG k-ϵ turbulence, RSM	Velocity vectors have been compared
Castilla et al.,2015 [10]	3D half pump and 2D all pump	Different 150 deforming mesh	Turbulence Model (it is not indicated which one)	Velocity change has been compared at a spot where is near to inlet region
Strasser,2007 [11]	2D	Deforming Mesh	Laminar, multiphase	-
Ackgoz[12]	3D all pump	Structured Mesh	RANS	Mass flow rate has been compared
Moilan et al., 2017[13]	3D half pump	Structure mesh and re-mesh after 1 degree rotation	k-ϵ, k-ω SST and RNG k-ϵ turbulence models	-

1.2 Observations

Numerical simulations of external gear pumps are hard task due to their complex geometries. The range of dimensions are from centimeters to micrometers. The number of cells of generated mesh are really high due to the clearance between tooth tip-body wall and the distance in gearing zone where the two gears are in contact and so, CFD (Computational Fluid Dynamics) analysis is not used too much as a design tool for external gear pumps. Therefore, simplified theoretical equations are still used for design of this type pumps. Theoretical leakage and volumetric displacement calculations are often performed in the literature with fully developed Couette flow assumptions [1, 5]. The fully developed flow is caused by the fact that the velocity distribution does not change during the flow due to the fact that the viscous forces are in balance with the other forces. The validation of these assumptions is an important information for those who design and analyze these equations. Theoretical validity of theoretical leakage and volumetric displacement analysis with CFD simulations should be examined quantitatively. Because, the numerical simulations will help to observe the theoretical calculation and the limits of the theory by providing a more detailed and precise examination of the flow inside the pump.

Overset unstructured mesh method can be used as a mesh model. But, mesh deformation is the main disadvantage of this method as mentioned in literature [14, 15, 16]. The solution of this problem is re-generation of mesh. However, re-generation of mesh makes the computational time higher and higher. Complex geometry and the range of dimensions complicates that using overset mesh method for numerical simulations of external gear pumps.

In the literature, temperature change on the body wall due to friction between teeth and wall has not been indicated so far. Indeed, temperature is another factor causing increase of tip leakage and need to be observed.

1.3 Hypothesis

Theoretical leakage and volume displacement analysis has to be verified numerical simulations. Numerical simulations help to examine theoretical calculation and limits of the theory. Theoretical leakage and volume displacement calculations are mostly performed with assumptions such as fully developed flow in literature. Validity range of the theoretical calculations can be examined in 2D numerical simulations by studying the flow structures and flow characteristics. Furthermore, temperature effect which can be occurred due to friction on the pump body decrease dynamic viscosity of fluid and increase tip leakages.

1.4 Methodology

3D unsteady CFD simulations require a lot of resources. In this study, a new 2D CFD analysis method which uses less resources has been developed in order to examine the tooth tip leakage in detail. The validity, flow structures and flow characteristics of the theoretical calculations are examined with this method. At the same time, a few 3D simulations have been performed to validate developed new 2D CFD analysis method.In developed new method, the gear pump geometry includes only the region which is between gear teeth and the pump body for one gear and two reservoirs as inlet and outlet volume packages, horizontally . Method will be explained in detail on next chapters. Furthermore, temperature effect was demonstrated by changing temperature wall in the 2D numerical simulations.

1.5 Thesis Structure

In this thesis, Chapter 2 presents theoretical equations for tip leakage, face leakage, gearing zone leakage and basics of numerical modeling. Chapter 3 shows comparison of theoretical calculations and 2D numerical simulations' results. Chapter 4 deals with 3D numerical simulations. In third and fourth chapters, problem statement,

numerical setup which includes computational domain, mesh conditions and boundary conditions, results are described and discussed. Finally, conclusions are at the end of thesis as Chapter 5.

CHAPTER II

THEORETICAL EQUATIONS

2.1 Reynolds Transport Theorem Equations

Reynolds transport theorem is used to compute derivative of integrated quantities. General form of the theorem is expressed as follows;

$$\frac{dB_{sys}}{dt} = \frac{\partial}{\partial x}\int_{CV} \rho b dV + \int_{CS} \rho b \vec{U}.\vec{n} dA \tag{1}$$

B is any arbitrary extensive property, b is the extensive property per unit mass, density ρ, velocity $\vec{U}$, and normal vector on the control surface $\vec{n}$, V is volume and A is the area. First term and second term at right-hand side represents rate of change of B within CV (Control Volume) and net flow rate of B through CS (Control Surface) respectively.

2.1.1 Conservation of Mass

It is also called "continiuty equation" . Mass M is the extensive property and expressed as;

$$B = M \tag{2}$$

so, b (extensive property per unit mass) equals;

$$b = \frac{B}{M} = \frac{M}{M} = 1 \tag{3}$$

By implementing general form of transport equation, conservation of mass is as follows;

$$\frac{\mathrm{d}M_{sys}}{\mathrm{d}x} = \frac{\partial}{\partial t}\int_{CV} \rho dV + \int_{CS} \rho \vec{U}.\vec{n} dA = 0 \tag{4}$$

i.e

$$\underbrace{\frac{\partial}{\partial t}\int_{CV}\rho dV}_{\text{rate of change of mass in CV}} + \underbrace{\int_{CS}\rho\vec{U}.\vec{n}dA}_{\text{net rate of mass flux through the CS}} = 0 \tag{5}$$

Let's assume ρ = constant as incompressible;

$$0 = \rho\frac{\partial}{\partial t}\int_{CV} dV + \rho\int_{CS}\vec{U}.\vec{n}dA \tag{6}$$

V is also constant and the first term on the right-hand side equals to zero;

$$0 = \underbrace{\rho\int_{CS}\vec{U}.\vec{n}dA}_{\text{volume flow rate}} \tag{7}$$

Equation(8) shows that net volume flow rate should equal to zero through CS. This equation is also valid for both of unsteady and steady flows.

2.1.2 Conservation of Momentum

Momentum $\vec{P}$ is the extensive property and defined as;

$$B = \vec{P} \tag{8}$$

so, b extensive property per unit mass is;

$$b = \frac{B}{M} = \frac{\vec{U}.M}{M} = \vec{U} \tag{9}$$

By implementing general form of transport equation, conservation of momentum is as follows;

$$\frac{\mathrm{d}\vec{P}}{\mathrm{d}t}_{system} = \frac{\partial}{\partial t}\int_{CV}\vec{U}\rho dV + \underbrace{\int_{CS}\vec{U}\rho\vec{U}.\vec{n}dA}_{\text{momentum flux}} \tag{10}$$

The change of momentum is also equals to forces acting on system. It can be expressed as;

$$\frac{\mathrm{d}\vec{P}}{\mathrm{d}t}_{system} = \vec{F}_{system} \tag{11}$$

Equation (12) shows that the sum of net rate change of momentum in control volume and net rate of momentum flux though control surface equals to all forces acting on system. The sum of body forces and surface forces equals to all forces acting on system. It is expressed as;

$$\vec{F}_{system} = \vec{F}_{body} + \vec{F}_{surface} \tag{12}$$

Surface forces mainly due to pressure and viscous stress. Pressure forces are normal to the surface and viscous stresses can be normal or tangential to surfaces. Besides, body forces are beacuse of magnetic field or gravity [17].

$$\vec{F}_{pres} = -\int_A P\vec{n}dA \tag{13}$$

$$\vec{F}_{vis} = \int_A \tau dA \tag{14}$$

2.1.3 Conservation of Energy

Energy E is the extensive property and expressed as;

$$E = B \tag{15}$$

then, b is the extensive property per unit mass;

$$b = \frac{B}{M} = \frac{E}{M} = e \tag{16}$$

By implementing general form, the conservation of energy is defined as;

$$\frac{\mathrm{d}E}{\mathrm{d}x}_{system} = \frac{\partial}{\partial t}\int_{CV} e\rho dV + \int_{CS} e\rho\vec{U}.\vec{n}dA \tag{17}$$

at initial t, the equation is;

$$\frac{\mathrm{d}E}{\mathrm{d}x}_{system} = \left|\dot{Q} + \dot{W}\right|_{system} = \left|\dot{Q} + \dot{W}\right|_{CV} \tag{18}$$

thus, the energy equation can be written in integral form as follows;

$$\left|\dot{Q} + \dot{W}\right|_{CV} = \frac{\partial}{\partial t}\int_{CV} e\rho dV + \int_{CS} e\rho\vec{U}.\vec{n}dA \tag{19}$$

2.2 Theoretical Leakage Equations

In this section, the leakages which are moving fluid from inlet to outlet through clearances in the pump are explained theoretically. Leakages in external gear pump are classified as tip leakage, face leakage and gearing zone leakage.

2.2.1 Tip Leakage

The working gap between tooth tip and body wall must be existed for design of external gear pumps. The fluid can leaks due to pressure difference from this gap. This leakage is called as "tip leakage". If the working gap is selected more than optimum value, it makes leakage from high pressure region to low pressure region higher [1]. Therefore, the performance of the pump and volumetric efficiency is affected negatively.

The unit flow element between tooth tip and wall at "h" clearance has been shown on Figure 1 and the flow resembles to Couette flow. The force balance on this element can be expressed as;

$$\frac{\mathrm{d}P}{\mathrm{d}x} = \frac{\mathrm{d}\tau}{\mathrm{d}y} \tag{20}$$

For Newtonian fluids, τ is defined as;

$$\tau = \eta\frac{\mathrm{d}u}{\mathrm{d}y} \tag{21}$$

Velocity change can be found by integrating equation 21 and 22 when the boundary conditions are u=0 for y=0 and u=U_{max} for y=h;

$$U = \frac{1}{2\eta}\frac{\mathrm{d}P}{\mathrm{d}x}\left(y^2 - hy\right) + \frac{y}{h}U_{max} \tag{22}$$

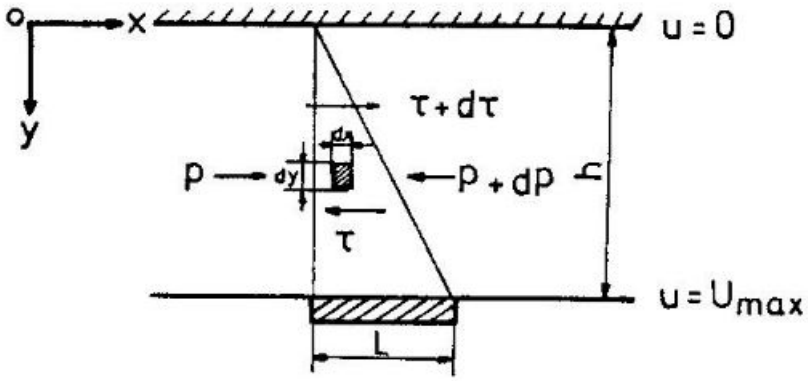

Figure 1: Forces acting on the unit flow element [1]

The amount of fluid between tooth tip and wall at the tooth with b width and moving U velocity can be found as follows;

$$Q = \int_0^h b\,u\,dy \tag{23}$$

By integrating equation 21;

$$Q = b\left(\frac{h\,\omega\,r_d}{2} - \frac{h^3\Delta P}{12\eta\,L}\right) \tag{24}$$

the amount of fluid from a tooth tip to outlet can be obtained. If equation 25 is arranged again, the statement of the amount of fluid which leaks from tooth tip to inlet is found as;

$$Q_{t.k} = b\left(\frac{h^3\Delta P}{12\eta\,L} - \frac{h\,\omega\,r_d}{2}\right) \tag{25}$$

b is tooth width, h is film thickness, ΔP is pressure difference, η is dynamic viscosity, L is top land and ω is angular velocity. The first term represents the amount of fluid moving back to inlet due to pressure difference and the second term represents the fluid which is moved to outlet by viscous adhesion to tooth tip.

Equation 26 calculates tip leakage through one tooth which is contact with wall. If there are more tooth in contact with wall, the equation can be expressed as;

$$Q_{t.k} = b\left(\frac{h^3 \Delta P}{12\eta\, L\, N} - \frac{h\,\omega\, r_d}{2}\right) \tag{26}$$

N is the number of teeth in contact with wall.

2.2.2 Face Leakage

The working gap between gears' faces and body face must also be existed for design of external gear pumps as mention before tip leakage section. This gap causes moving fluid from outlet side to inlet side due to pressure difference and the leakage is called "face leakage".

Koc and Canbulut[1] has been investigated face leakage by seperating the gear couple to two regions and it is showed Figure 2. When the direction of movement of the gear is taken into account, although it was in the first region in the direction of the leakage resistance, the leakage is correlated with the direction of movement of the second region.

U_0 and $h(r_d - r_m$ are the velocity of gear and the section of moving fluid respectively. r_m is radius of shaft, r_o average radius and $r_d - r_m = b$, $L = \pi.r_o$ for first region;

$$Q_I = \int_0^h b\, U_0\, dy \tag{27}$$

is expressed and if equation 22 is used for U_0 and integrate to equation 27 with multiplying minus to calculate the leakage at first region;

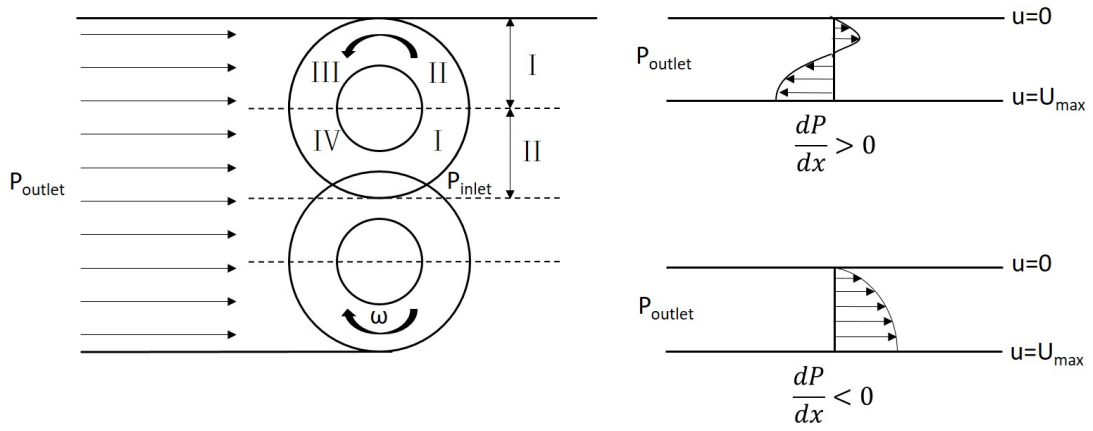

Figure 2: Characteristic regions on lateral faces of gear pump according to Koc and Canbulut [1]

$$Q_{y,k,I} = b\left(\frac{h^3 \Delta P}{12\,\eta\,L} - \frac{\omega\, r_o\, h}{2}\right) \tag{28}$$

is obtained.

For second region, the direction of movement is the same with the direction of leakage. Therefore, second term in equation 28 must be added to first term. So, the statement of face leakage can be defined as;

$$Q_{y,k,II} = b\left(\frac{h^3 \Delta P}{12\,\eta\,L} + \frac{\omega\, r_o\, h}{2}\right) \tag{29}$$

2.2.3 Gearing Zone Leakage

In external gear pumps, instantaneous pressure drop is observed at the contact area of driving and driven gear because of squeezing the fluid too much. This causes that the fluid leaking from contact area to inlet region . This leakage called as "gearing zone leakage".

Koc and Canbulut[1] calculates the gearing zone leakage as follows;

$$Q_{y,k,m} = b\left(\frac{h^3 \Delta P}{12\,\eta\,L} + 2\,\frac{\omega\, r_d\, h}{2}\right) \tag{30}$$

CHAPTER III

NUMERICAL MODELING

In this section, numerical modeling has been separated as 2D numerical modeling and 3D numerical modeling. The geometry, mesh generation, boundary conditions and physics models have been explained in detail in these subsections.

Numerical simulations were performed on Star-CCM+. STAR-CCM+ can simulate internal and external fluid flow across a wide range of flow regimes, and for a variety of fluid types. It solves the conservation equations for mass, momentum, and energy for general incompressible and compressible fluid flows. Star-CCM+ uses finite volume method on numerical simulations. These equations is defined respectively as follows;

$$\frac{\partial}{\partial t}\left(\int_V \rho\, dV\right) + \oint_A \rho\, \mathbf{v_r}.d\mathbf{a} = \int_V S_u dV \tag{31}$$

ρ is density, v is velocity and S_u is mass source for unit volume.

$$\frac{\partial}{\partial t}\left(\int_V \rho\, \mathbf{v} dV\right) + \oint_A \left(\rho\, \mathbf{v_r} \otimes \mathbf{v}\right).d\mathbf{a} = -\oint_A p\mathbf{I}.d\mathbf{a} + \oint_A T_v.d\mathbf{a} - \int_V \rho\left[\omega \times (\mathbf{v} - \mathbf{v_t})\right] dV + \int_V f_b dV \tag{32}$$

$\otimes$ is Kronecker multiplier, p is pressure, T_v is viscous stress tensor and fb is resultant body forces acting on unit volume.

$$\frac{\partial}{\partial t}\int_V \rho\, E dV + \oint_A \left[\rho H \mathbf{v_r} + \mathbf{v_g} p\right].d\mathbf{a} = -\oint_A \dot{q}''.d\mathbf{a} + \oint_A T_v.\mathbf{v}d\mathbf{a} + \int_V \mathbf{f_b}.\mathbf{v}dV + \int_V S_E.dV \tag{33}$$

E is total energy in unit mass, q is heat flux and S_E is energy source in unit volume [18].

3.1 2D Numerical Modeling

Numerical simulation of external gear pump is too hard and time-consuming task due to close gaps. These gaps cause low mesh size, high number of mesh cells and too long computational time in numerical simulations. Especially, 3D numerical simulations cannot be done for all geometry of external gear pump as is seen on Table 1. In this study, 3D numerical simulations have been tried to perform for a section of proposed external gear pump; but it could not be completed due to not enough source and overset mesh method. Therefore, 2D numerical simulations has been performed with developed new method. In addition, 3D numerical simulations has been done with moving reference method for a section of gear pump.

To decrease number of mesh cells and computational time, the geometry of gear pump is simplified for numerical simulations in this study. The geometry conversion is shown on Figure 3. The geometry scene of flow domain including two reservoirs and 10 teeth in contact with the wall is shown in Figure 3. This simplified geometry has been created based on radius of gear. The dimensions of flow domain are given on Table 2. In fact, each gear has 14 teeth; but 10 teeth are investigated in this study. Because tip leakages are observed only in the region which is in contact with wall and includes 10 teeth. The dimensions of geometry are given at Table 2.

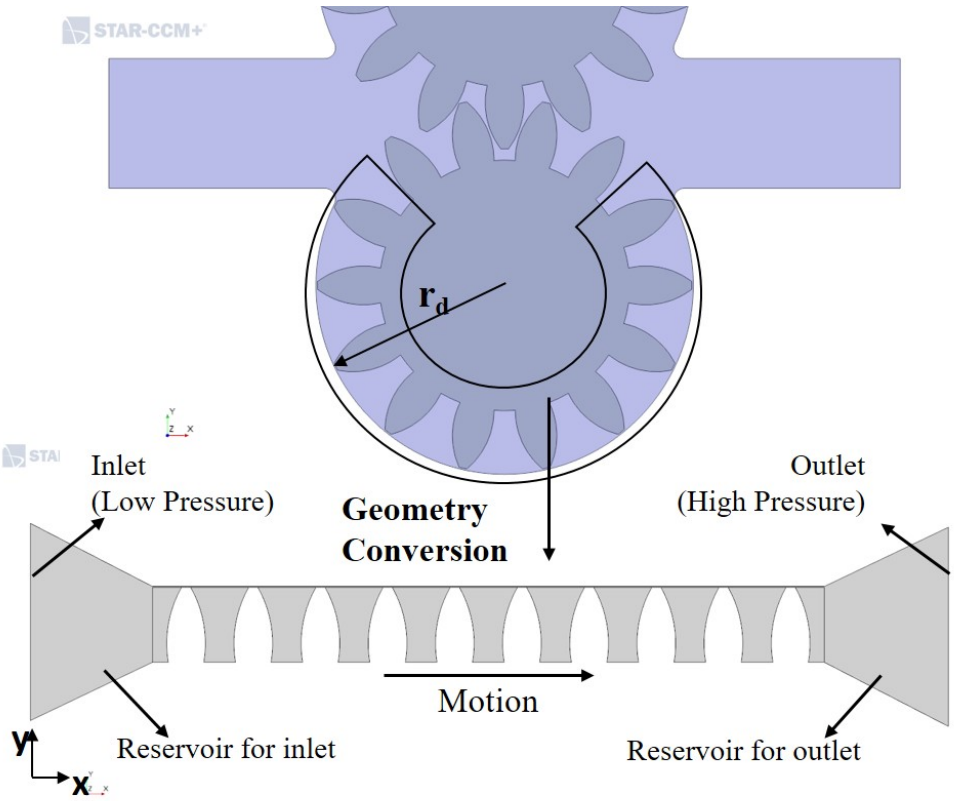

Figure 3: Geometry conversion and geometry scene of fluid domain

Table 2: Flow Domain Dimensions in 2D numerical simulation

Symbol	*Definition*	*Unit*	*Dimension*
h	Film Thickness	μm	36.3
b	Face width	mm	4.5
L	Top Land	mm	0.371
r_d	Radius of Gear	mm	8.69

The flow is modeled as incompressible and laminar. Water is used as fluid. Properties of water are shown on Table 3. Second order implicit unsteady solver has been used for numerical simulations. Time step has been adjusted 0.1 μs. In addition, inlet and outlet boundaries have been modeled pressure inlet and pressure outlet. The

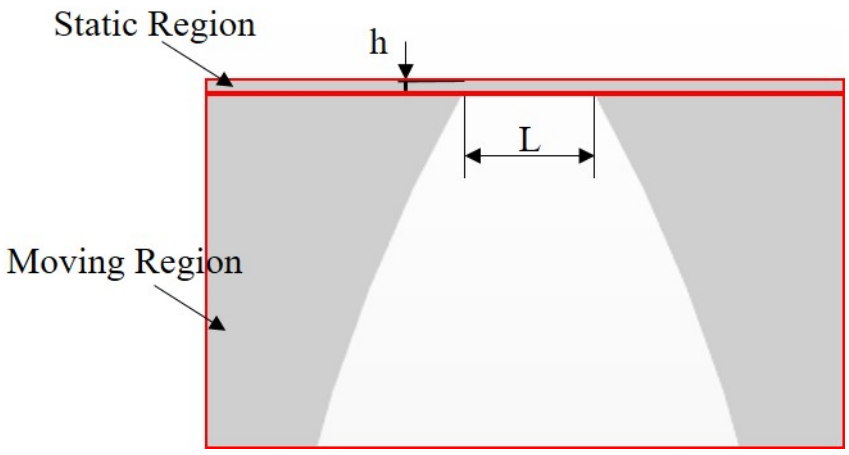

Figure 4: Geometric dimensions of fluid domain and moving and static regions

remaining boundaries have been modeled wall. Reference pressure and inlet pressure are given as 1 bar and 0 bar respectively. Outlet pressure is given 2, 5, 8, 10 bar as gauge pressure. In addition, the translation velocity has been calculated through rotation speed and radius of gear. Rotation speeds are 400, 600, 800, 1000, 1200, 1400, 1600 rpm. There are two regions as moving body and fixed body. Moving body includes gear teeth and volume packages. Moving frame to x+ direction is defined to moving body by using translation reference frame. Besides, fixed body contains two reservoirs and the surface between gear teeth and wall. In numerical simulations, since the pump is drawn horizontally as described above, the translation speed corresponding to each rotation speed is calculated and these speeds are defined respectively for the moving region.

Table 3: Properties of Water

Symbol	*Definition*	*Unit*	*Dimension*
ρ	Density	kg/m^3	997.56
η	Dynamic Viscosity	Pa.s	$8.8871.10^{-4}$

Part based meshing has been used for mesh generation on Star-CCM+. An unstructured 2D polyhedral mesh grid has been constructed for moving region and fixed region. Also, prism layer mesh has been used to observe more accurate results at zone close to wall, decrease the number of cells and computational time. Total number of cells is 106163 from which 38217 belongs to moving body and 67946 to fixed body. The mesh scenes of all fluid domain and between teeth tip and wall are shown in Figure 5 and Figure 6 respectively. Base size of mesh generations has been adjusted as 0.0001 m. Target and minimum surface size ,which specifies the face size that the mesher aims to achieve in the absence of smaller mesh controls and removes mesh edges below this size where feasible respectively, are given 100 and 10 as percentage of base. Surface growth rate, which specifies the maximum size ratio of connected mesh edges, is given as 1.3 . Prism layer mesher is also used for mesh generation due to solve more accurate at critical points, surfaces such as next to walls. Furthermore, there are three surface control in the mesh operation. First surface control includes all surfaces at geometry except for teeth tips. Prism layer mesher is disabled at this control. Second one contains tooth tips to specify prism layer mesher and target surface size. Number of prism layers are 10, prism layer stretching, which specifies the thickness of each cell layer as a ratio of the previous layer, is 1.1 and total thickness of prism layer mesher is 30 μm . The third control involves tooth tip too. But, target surface size is controlled and given 0.5 as percentage of base.

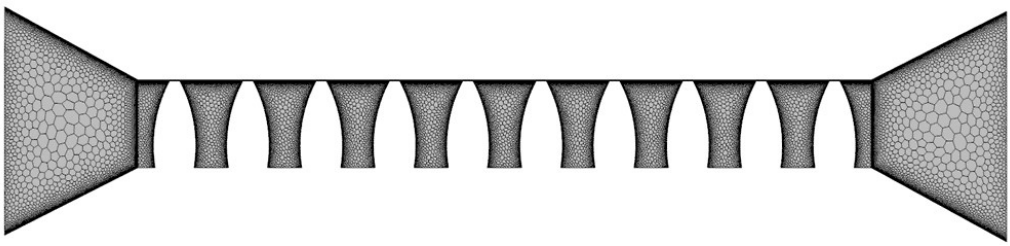

Figure 5: Mesh scene of all fluid domain (2D)

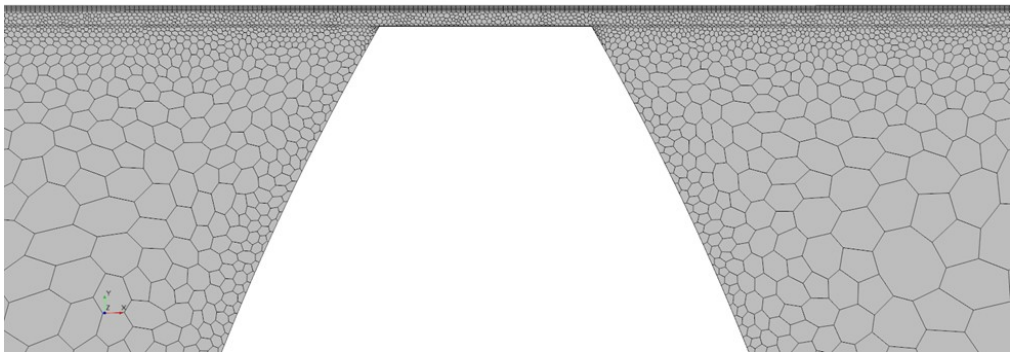

Figure 6: Mesh scene between teeth and wall (2D)

In this study, mesh dependency has been done for 2D numerical simulations in case 5 bar 1400 rpm. The total number of mesh cells are 63819, 76971, 106163, 162406 and 207891 respectively. Tip leakages and velocity vector between middle tooth tip and wall have been investigated. In Table 11, tip leakages increase a few, as the number of mesh cells rises. This increase can arise from the higher number of cells between tooth tip and wall. However, there is a high difference from theoretical tip leakage calculations. Velocity profiles has been observed to see whether fully developed flow exist or not at middile tooth. Nineteen plane sections has been created between wall and middle tooth and tenth plane section is middle one on tooth. In Figure 7, velocity profiles at tenth plane section between tooth tip and wall for different number of mesh cells are shown. As total number of cells increase, the flow form is closer to fully developed flow. Nevertheless, theoretical calculated maximum velocity is three times lower than 2D numerical simulations which total number of cells is 207891.

Table 4: Tip leakage for different number of mesh cells in case 5 bar-1400 rpm

Number of Mesh Cells	*Tip Leakage* (kg/s)
63819	0.00163
76971	0.00165
106163	0.00171
162406	0.00175
207891	0.00179

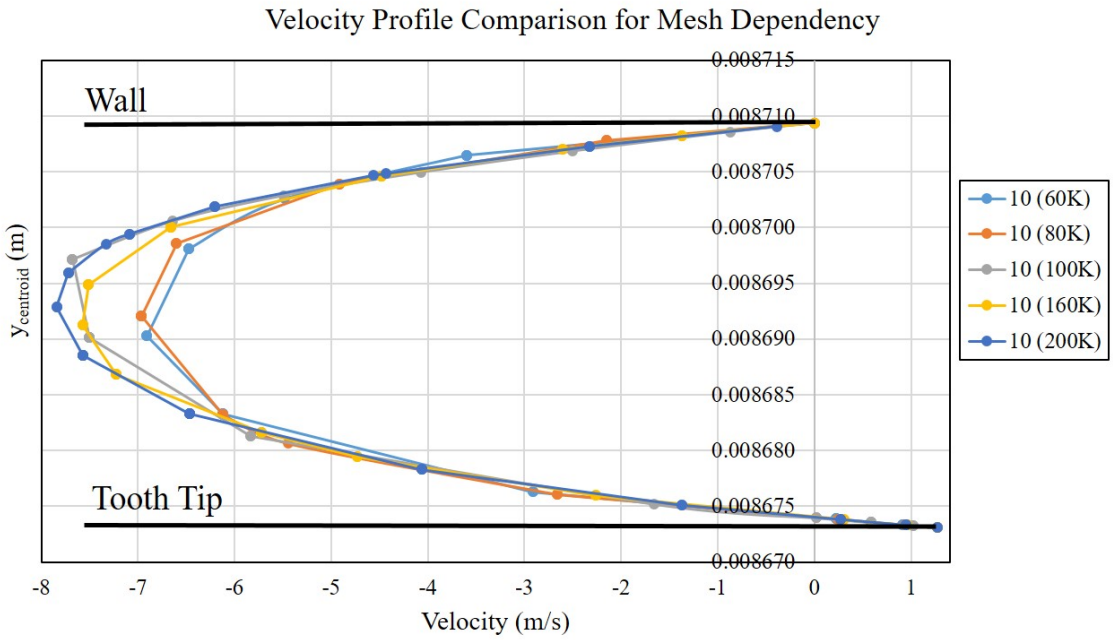

Figure 7: Comparison of velocity profile at tenth plane section in 2D between tooth tip and wall for different number of mesh cells

Temperature change at body wall due to friction between wall and teeth tips have been investigated in 2D numerical simulations. Because of too long computational

time of 3D numerical simulations, this subject couldn't be investigated as 3D. Temperature specification of body wall has been changed as "temperature" and given 303 K, 313 K, 323 K, 333 K respectively. In addition, dynamic viscosity property of water was used as a polynomial function in T between $5 - 95°C$ as below;

$$\eta = 2.4857.10^{-11}.T^4 - 3.4276.10^{-8}.T^3 + 1.7779.10^{-5}.T^2 - 4.1167.10^{-3}.T^1 + 0.35987 \tag{34}$$

3.2 3D Numerical Modeling

3D numerical simulation of external gear pump needs high performance computing because of excessive number of mesh cells on complex geometry of the pump. Table 1 shows that half geometry or the geometry which includes inlet chamber and several teeth have been used in numerical simulations. Furthermore, moving mesh methods has been used such as adaptive mesh method or overset "chimera" mesh method due to moving boundaries. However, these methods require re-generation of mesh due to deforming mesh cells. Mesh re-generation causes that makes computational time higher.

In this study, overset mesh and moving reference frame method has been used to simulate the external gear pump as 3D.

3.2.1 3D Simulation with Overset Mesh

In this study, overset mesh method has been tried to simulate the flow inside of external gear pump. Overset mesh is most useful in problems dealing with multiple or moving bodies. In overset mesh, there should be mainly two type regions such as background region and overset region. Background region is the case of the gear pump; overset regions are gears. Overset regions should be created for each moving body. So, there are two overset regions due to including two gears in computational

domain. In addition, interfaces between each group of region must be created. Three interfaces has created in total such as overset (1)-background, overset (2)-background and overset (1)-overset (2). Interfaces provide transferring the flow variables by overlapped cells of each other. Overset mesh has three type cells as active, inactive and acceptor cells. When overset region moves, acceptor cells provide flow of information to active cells. In addition, cell types can change from one to other. However, overset mesh has a significant disadvantage for numerical simulation of external gear pump. When the gears rotates, mesh cells are deformed due to geometry of pump. Therefore, some cells are disappeared and the flow of information between cells cannot carried to each other. Thus, the simulation explodes and cannot reach a solution.

The geometry of fluid domain is shown on Figure 8. The gears has 22 teeth and the radius of gears are 23.37 mm. Film thickness, which is distance between tooth tip and wall, is 100 μm. Although the actual thickness of pump is 10 mm, the thickness in numerical simulations is 0.2 mm to reduce the computational time and number of mesh cells. Top land of tooth is 1.17 mm.

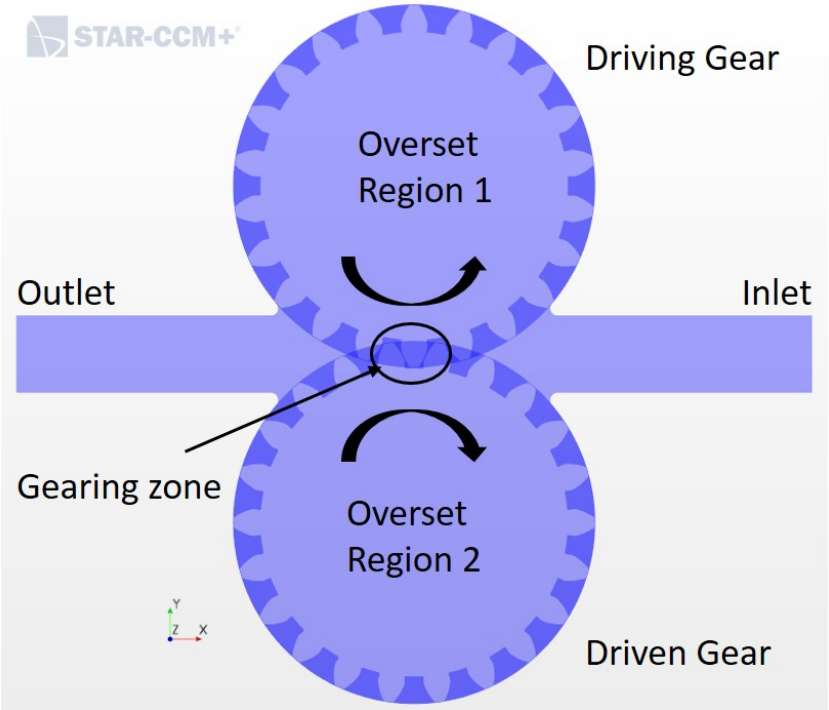

Figure 8: Geometry scene of fluid domain (3D simulation with overset mesh)

The flow is modeled as laminar. Cavitation model is activated due to instantaneous pressure drop at gearing zone. Therefore, Eulerian multiphase model is selected and created liquid and vapor phases for water. Second order implicit unsteady solver has been used in this simulation. Time step has been adjusted 0.3 μs. Time step is too low due to keep the CFL number under 1. If CFL number increases more than 1, the simulation is crashed because of the fact that the flow of information passes through without solving some cells.

The boundary types of inlet and outlet has been selected as pressure inlet and outlet. Reference, inlet and outlet pressure are 1 bar, 0 bar and 2 bar respectively. Overlapped boundaries' types in overset and background regions must be the same to provide the flow of information between overlapped mesh cells. Due to the fact that the thickness of pump is not in actual dimension, top and bottom surfaces has been modeled symmetry plane for both of overset and background regions. The

remaining boundaries has been modeled wall. Rotation motions have been created for two overset regions as 300 rpm.

An unstructured parts based 3D polyhedral mesh grid has been constructed for overset regions and background region separately. Prism layer mesher has been used at gearing zone and between gear teeth-wall to generate more mesh cells and obtain more accurate solutions. Total number of cells is 693418 which 156161 belongs to overset region 2, 157097 to overset region 1 and 380160 to background region. The default controls of background and overset regions' meshes are shown on Table 4.

Surface and volumetric controls have been created to optimize the number of mesh cells and make the mesh better passing through from a region to another region. For background region, prism layer cells has been disabled in surfaces which is no need sensitivity for solution such as wall sides inlet and outlet chamber. In addition, volumetric control, which is called "refinement", has been created in background region to provide better mesh passing from overset to background (Figure 9). For overset region, any control type has not been used in the simulation. The all mesh scenes are shown on Figure 10-12.

Table 5: Default controls of Background and Overset Regions' Meshes

Default Controls	*Background*	*Overset*
Base Size (m)	0.002	0.0002
Surface Growth Rate	1.3	1.2
Target Surface Size (%)	100	100
Minimum Surface Size (%)	10	50
Number of Prism Layers	10	8
Prism Layer Streching Factor	1.1	1.1
Prism Layer Total Thickness(m)	0.0002	0.00009

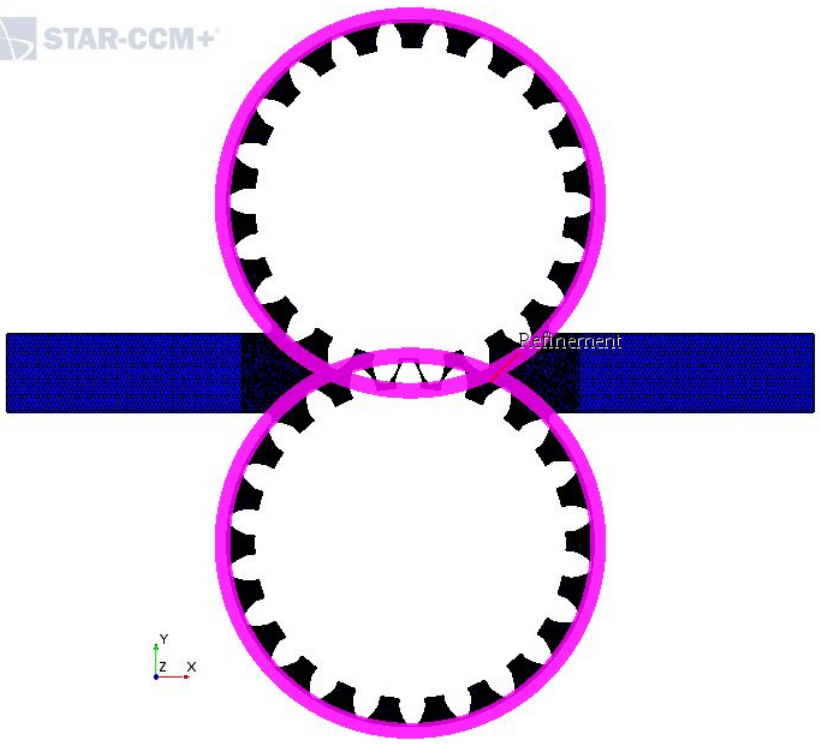

Figure 9: Volumetric control in background region (3D simulation with overset mesh)

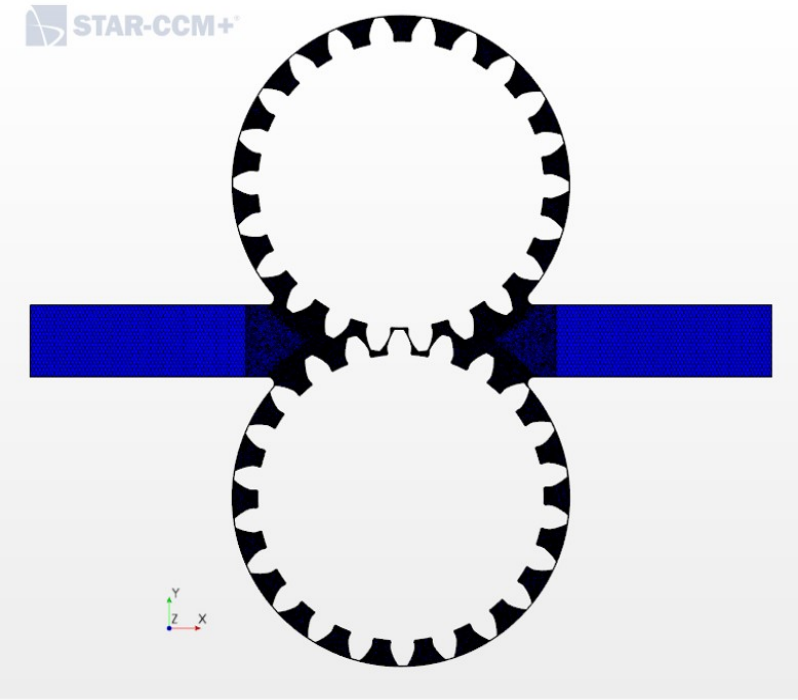

Figure 10: The mesh scene of all fluid domain (3D simulation with overset mesh)

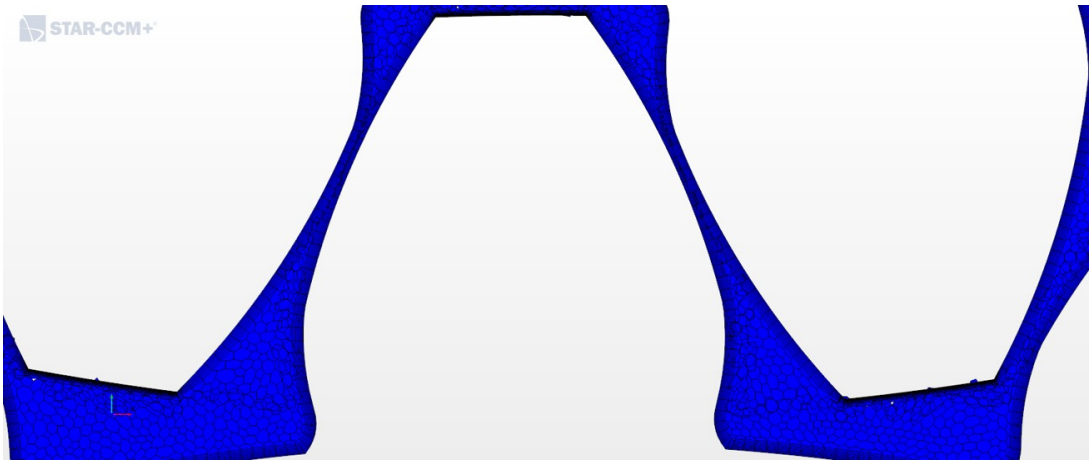

Figure 11: The mesh scene of gearing zone

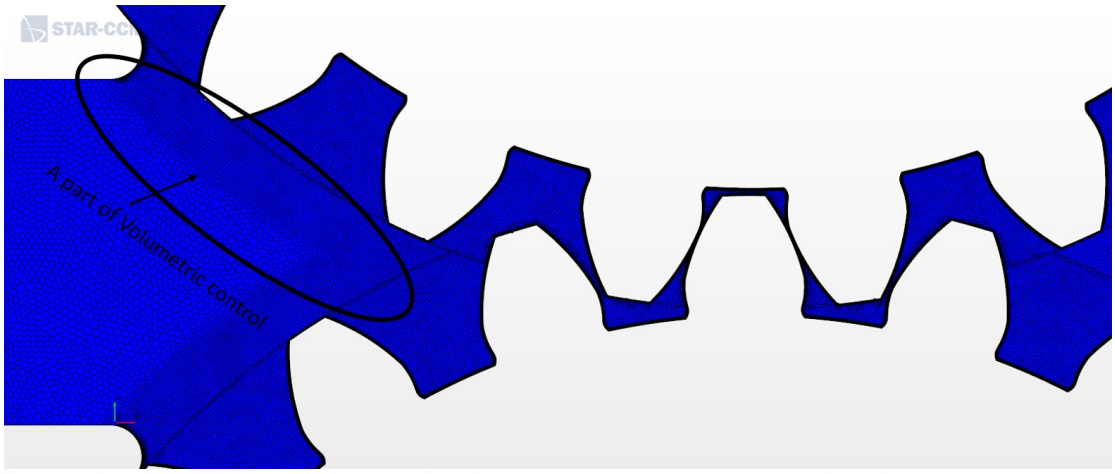

Figure 12: The mesh scene of refinement region and a part of outlet chamber (3D simulation with overset mesh)

The contact region of two gears are called "gearing zone" in this study. Instantaneous pressure drop and velocity change has been observed at gearing zone. It causes increase of CFL number dramatically. For this reason, CFL time step control modeled has been used on Star-CCM+. This option provides that CFL number remains under a value which is specified by user. The minimum time step and target mean CFL number and should be also determined. The model helps to control the time step with changing factor by specified minimum time step. But, the computational time increases when time step decreases. Due to that, a numerical method has been used as it is called Contact Zone. This method helps to decrease the velocity at gearing zone with increasing the viscosity artificially. Firstly, prism layer cells are defined as 0 or 1 by creating scalar field functions. If both gears have prism layer cells which are defined as 1, these cells are at Contact Zone. After that, the viscosity is increased dramatically and the velocity decreases for these cells. Furthermore, the leakages which are at gearing zone decreases at the same time. Surely, Contact Zone changes per time step by updated interfaces which are created for each group of regions such as overset-background, overset-overset.

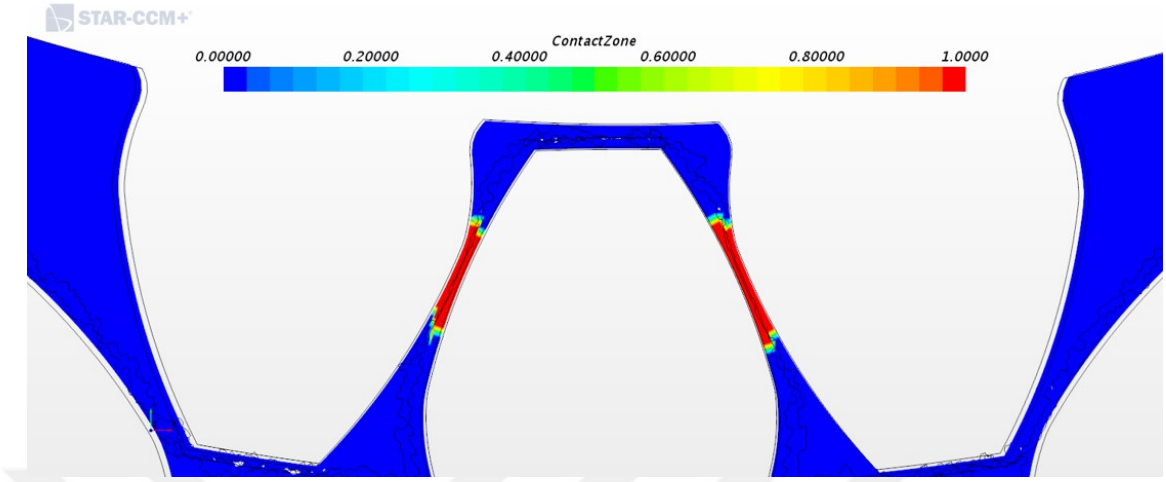

Figure 13: Scene of the contact zone method at gearing zone (3D simulation with overset mesh)

3.2.2 3D Simulation with Moving Reference Frame

Moving reference frame method has been used in numerical simulations, when the accurate and reliable solution couldn't be obtained from overset mesh method. In moving reference frame method, rotation motion is defined for moving boundaries as in overset mesh. However, moving boundaries and mesh cells are stable and does not rotate. Thus, there is no mesh deformation.

The geometric dimensions of external gear pump are the same with the geometry which is used in 2D numerical simulations (Table 2). The geometry scene is shown on Figure 14. In numerical simulations, half geometry of pump has been used as 2.25mm to reduce computational time and number of mesh cells.

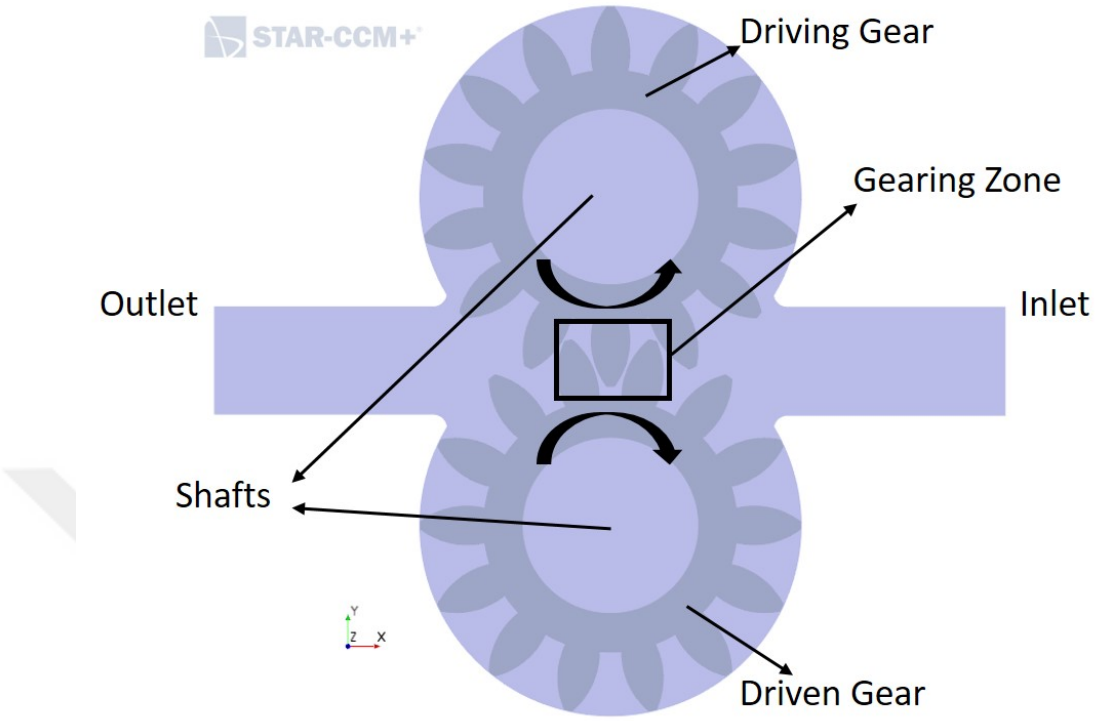

Figure 14: Geometry scene of fluid domain (3D simulation with moving reference frame)

The differences from other simulations are the shafts and the space between case and gears' faces. This space has been created to observe the face leakages for comparing with theoretical calculations (Figure 15) . Its dimension is 50 μm.

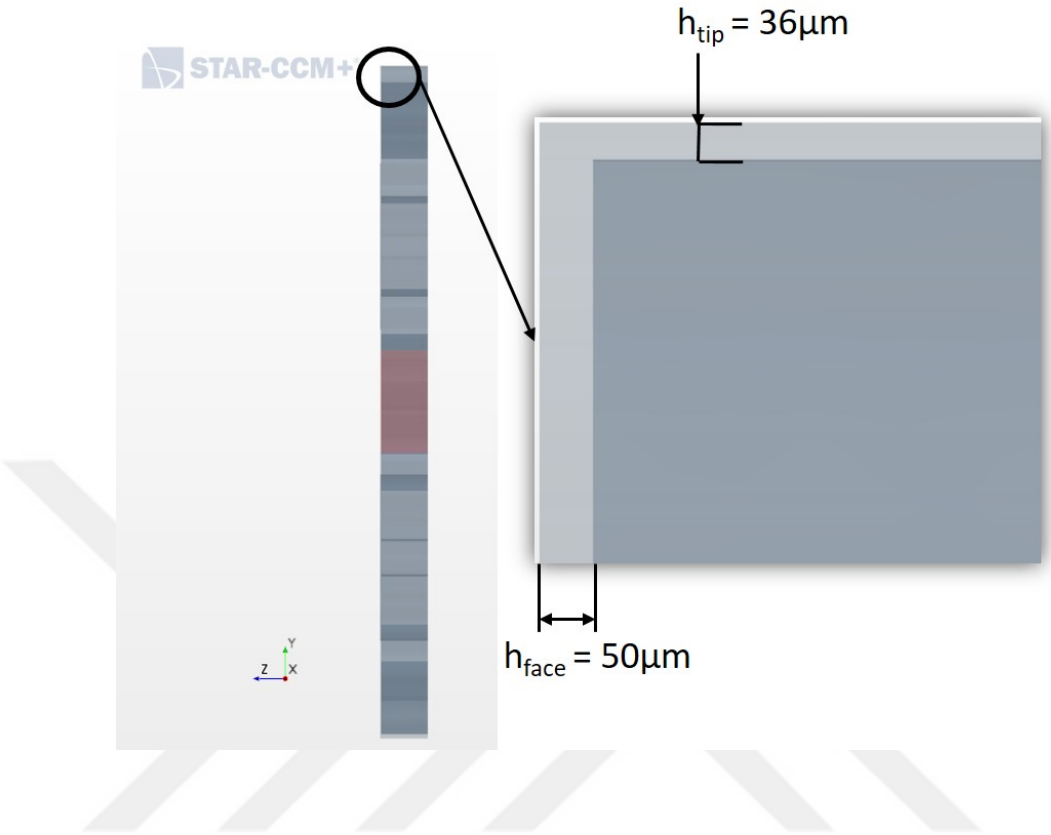

Figure 15: The space between case and gears' faces

Two different physics models are created separately as solid for gears and fluid for flow. The flow is modeled as laminar and Eulerian multiphase. Second order implicit unsteady solver has been used in the simulation as in 3D simulation with overset mesh method. Time step has been adjusted 0.1 μs. CFL number is important parameter in this method too. The maximum CFL number should be under 1 and so, time step has been given too low. This causes increasing the computational time too much. One simulation takes approximately one and half months.

The boundary types of inlet and outlet have been selected as pressure inlet and pressure outlet. The bottom boundaries of gears and case have been modeled as symmetry plane due to the fact that the fluid domain is half geometry of pump. Remaining boundaries are no-slip wall. Reference pressure and inlet pressure has been given as 1 bar and 0 bar respectively. Outlet pressure has been given 5 bar and

10 bar. Rotations motions have been created for gears. Rotation speeds are 1400 rpm for 5 bar and 800 rpm for 10 bar.

Parts based unstructured 3D polyhedral mesh grid has been generated in numerical simulations by using moving reference frame method. Prism layer mesher has been used between teeth tip-wall and gear faces-case face to obtain accurate results for tip leakage and face leakage. Total number of mesh cells are 4059494 which 466934 belongs to upper gear, 469004 to lower gear and 3123556 to case. The default controls of mesh are shown on Table 5 as follows;

Table 6: Default Controls of Mesh for Case and Gears

Default Controls	*Case*	*Gears*
Base Size (m)	0.001	0.0005
Surface Growth Rate	1.1	1.1
Target Surface Size (%)	80	100
Minimum Surface Size (%)	10	10
Number of Prism Layers	3	-
Prism Layer Streching Factor	1.1	-
Prism Layer Total Thickness(m)	0.00001	-

Surface and volumetric controls have been created for case to reduce and optimize the number of mesh cells as in 3D numerical simulations with overset mesh method. Prism layer cells have been disabled in surfaces which is no need precise solution such as side walls of case, inlet and outlet chamber. In addition, there are two volumetric controls as "refinement" and "gearing zone". These volumetric controls are shown on Figure 16. In this simulation, prism layer mesher has not been used at gearing zone. Instead, volumetric control which is called "gearing zone" has been created and adjusted custom size as 30 μm.

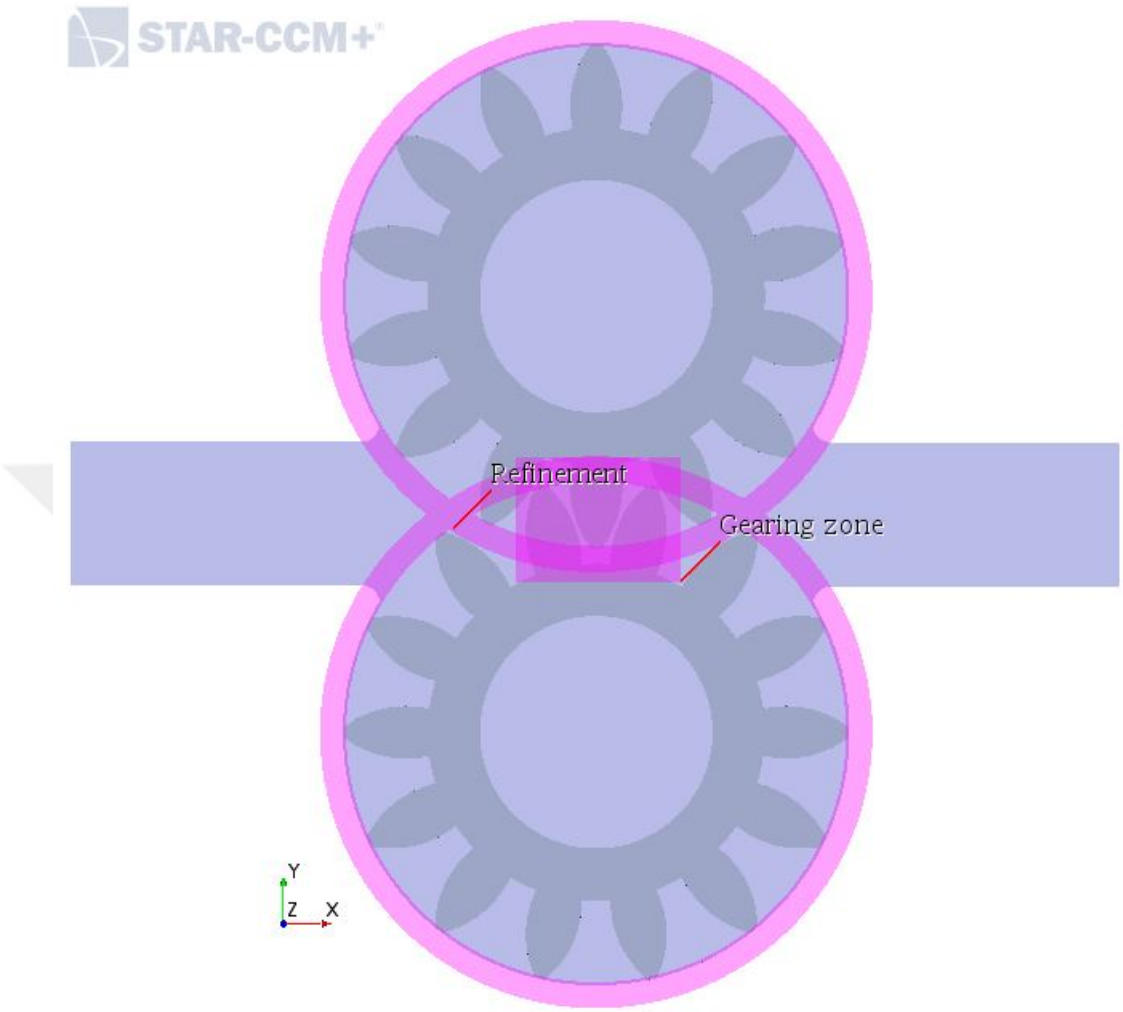

Figure 16: Volumetric controls; "Refinement" and "Gearing Zone" (3D simulation with moving reference frame)

The mesh scenes of all fluid domain, the region between gear face-case, gearing zone are shown Figure 17-19.

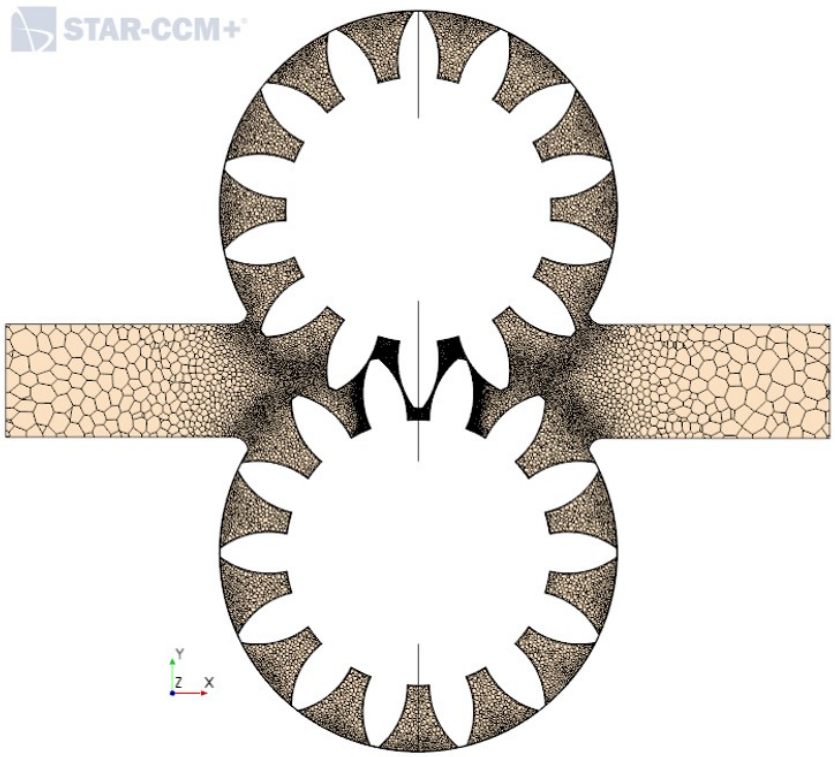

Figure 17: The mesh scene of all fluid domain (3D simulation with moving reference frame)

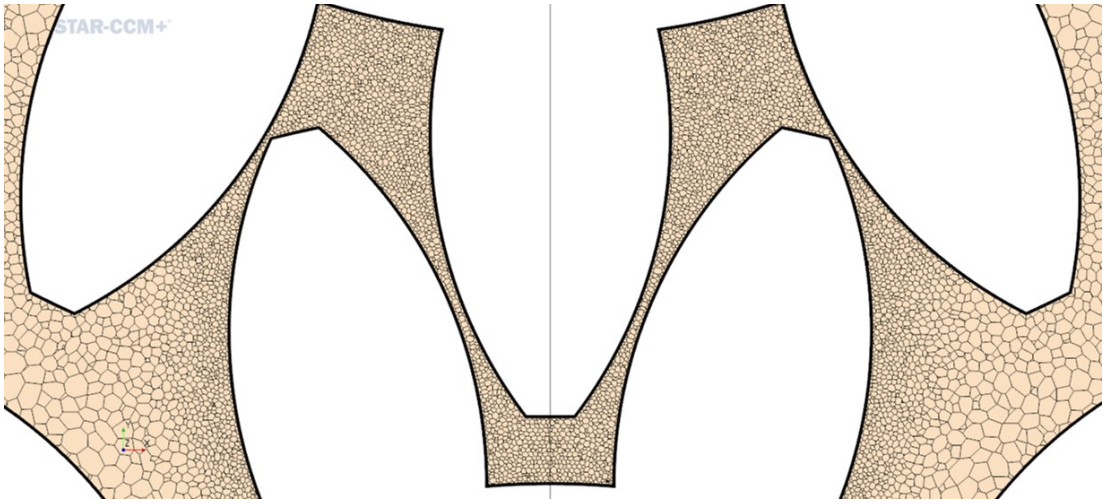

Figure 18: The mesh scene at gearing zone

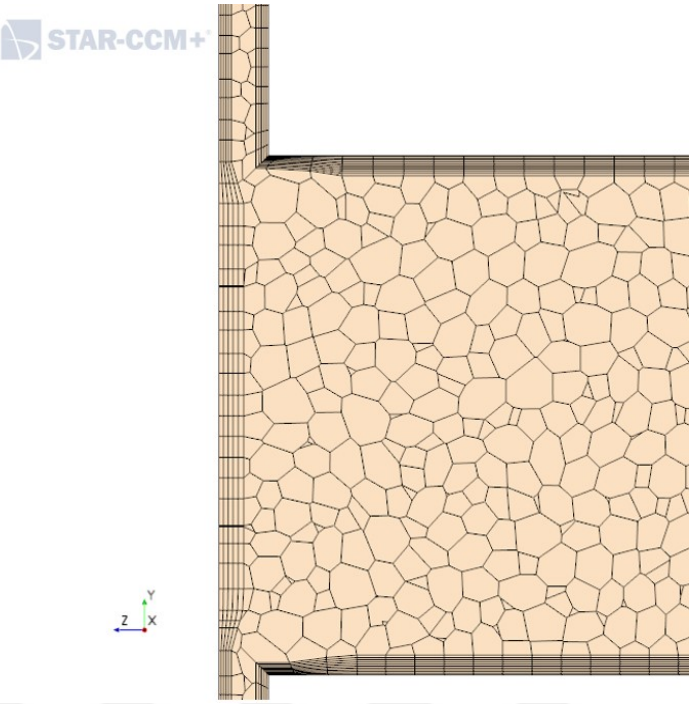

Figure 19: The mesh scene the space between gears' faces and case face (3D simulation with moving reference frame)

CHAPTER IV

RESULTS

In this section, theoretical calculations, 2D numerical simulations and 3D numerical simulations by using moving reference frame method have been compared and discussed. Furthermore, the causes of failure of 3D numerical simulation by using overset mesh method has been explained in detail.

4.1 Numerical Results of 3D Simulation by Using Overset Mesh Method

Vector scenes of the flow inside fluid domain is shown on Figure 20-21-22 when the pressure difference is 2 bar and rotational speed is 300 rpm at 50 ms.

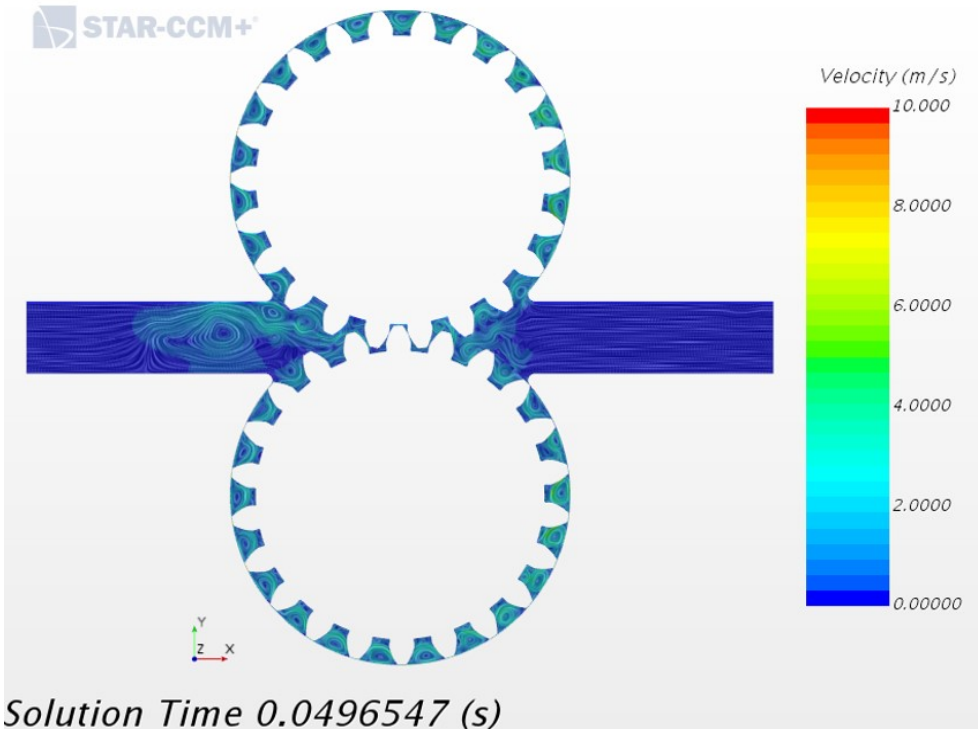

Figure 20: Vector scene of all fluid domain (3D simulation with overset mesh)

The fluid tries to go back from the space between teeth tip and case as gear rotates. However, volume packages, which is moved between teeth, push forward the leak fluid; so, the vorticities occur at volume packages (Figure 21).

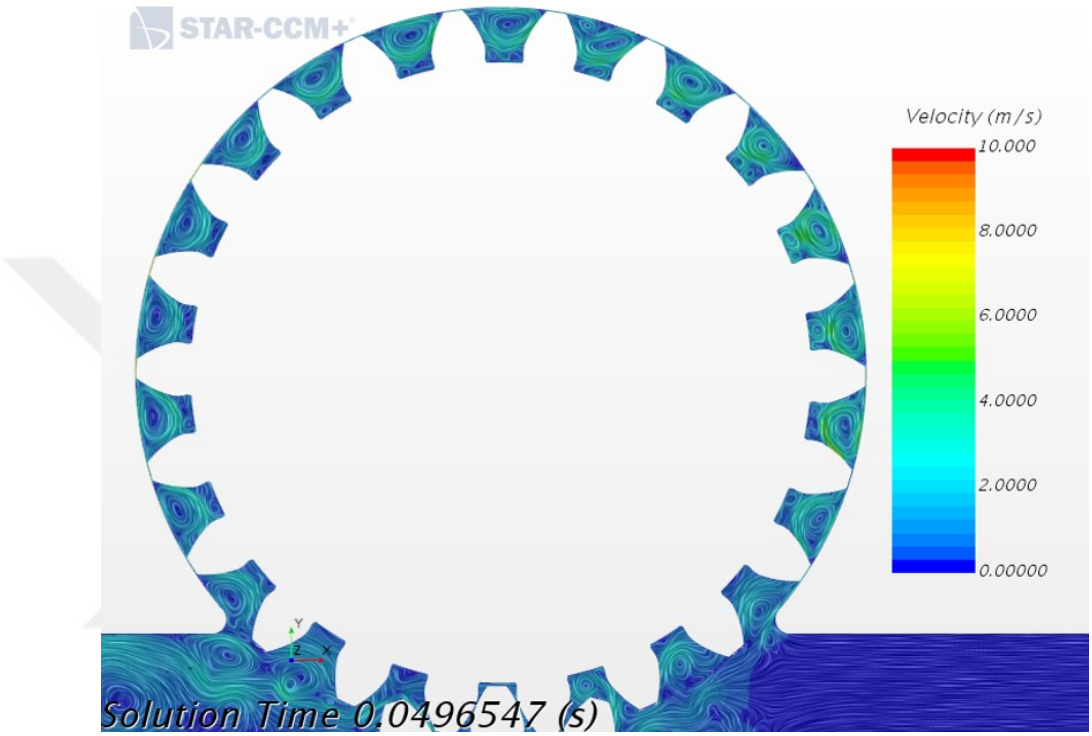

Figure 21: Vector scene of upper gear's volume packages(3D simulation with overset mesh)

"Contact zone" method has been used to prevent the problems caused by instantaneous pressure drop and velocity change, as mentioned before. Therefore, velocities has been reduced approximately $1m/s$ at gearing zone (Figure 22). Normally, the maximum velocities of the flow can be seen in contact area of driving and driven gears. In addition, the leak fluid can be observed as a path from outlet side to inlet side on Figure 22.

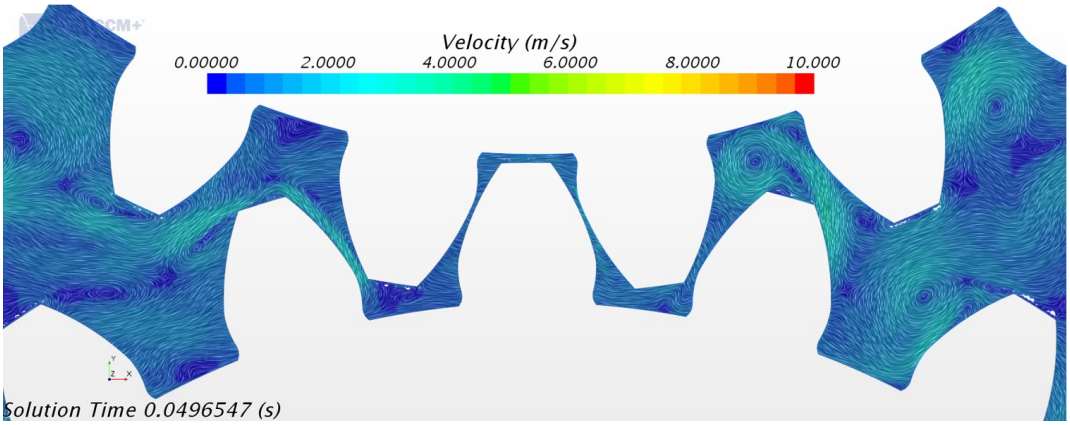

Figure 22: Vector scene at gearing zone(3D simulation with overset mesh)

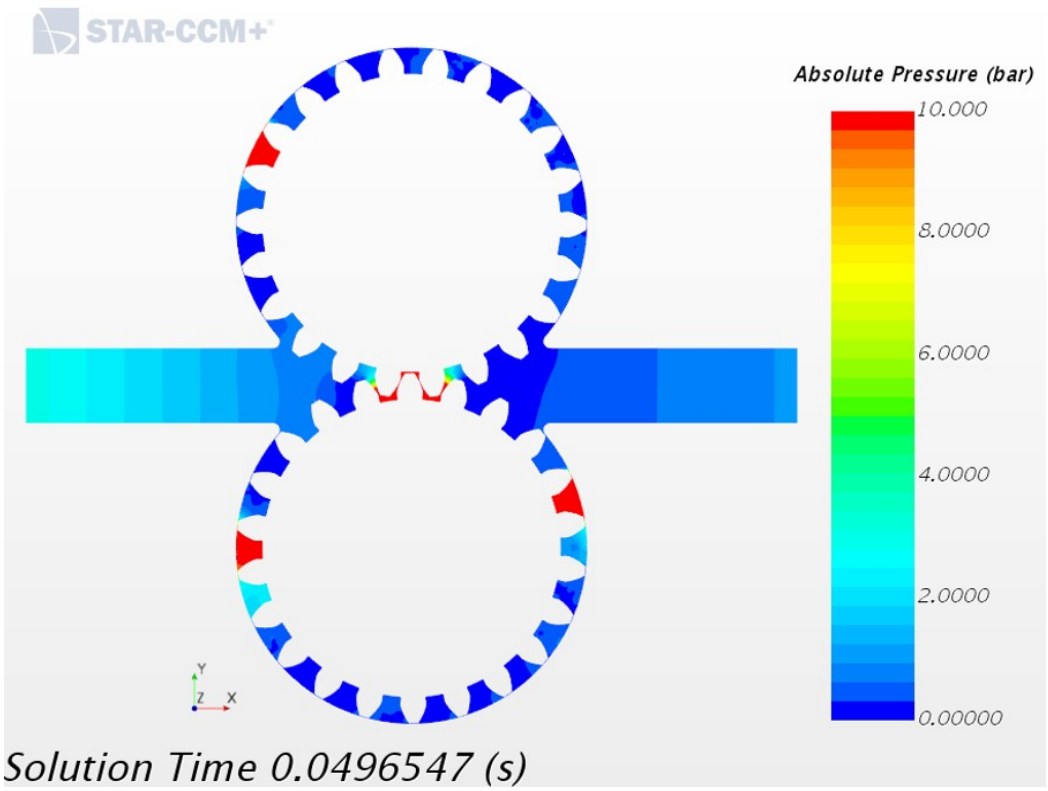

Figure 23: Pressure distribution of flow domain(3D simulation with overset mesh)

Pressure distribution in the flow domain are shown on Figure 23 and Figure 24.

Pressure difference between inlet and outlet is 2 bar as adjusted at boundary conditions. However, there are some unexplained problems in volume packages of upper and lower gears. Pressure in volume packages at the red zones is approximately 40 bar. Furthermore, these red zones has been changed almost at every time step. It may be caused by "Contact zone" method, but it has been observed the cases which are not used "Contact Zone" method. In fact, pressure must be increase gradually after each teeth from inlet to outlet.

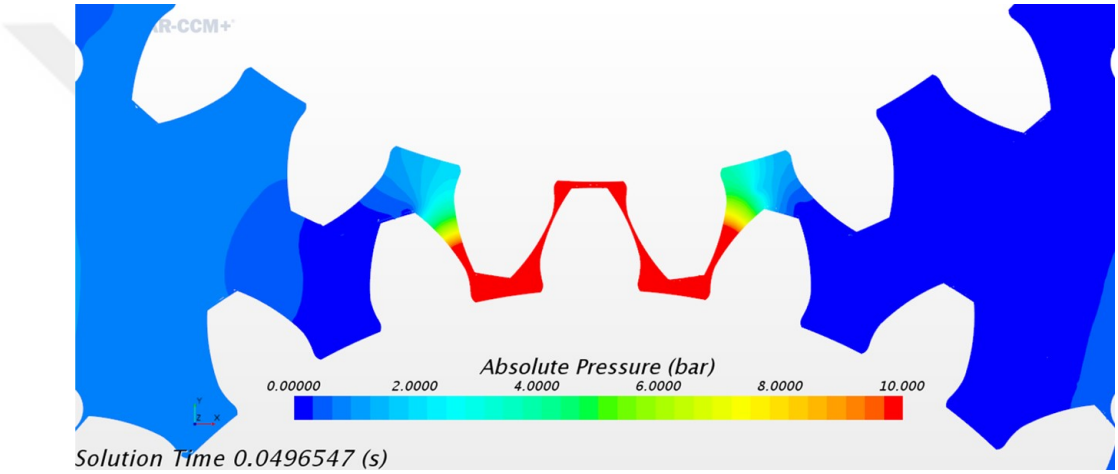

Figure 24: Pressure distribution at gearing zone(3D simulation with overset mesh)

The another important matter in this simulation is maximum CFL number in fluid domain. As mentioned before, CFL number must be kept under 1 in all fluid domain. The following chart shows that this matter is achieved by adjusting the sufficient time step. Maximum CFL number value is 0.5 on average and approximately 0.95 as maximum and 0.2 as minimum. The CFL number chart are shown on Figure 25.

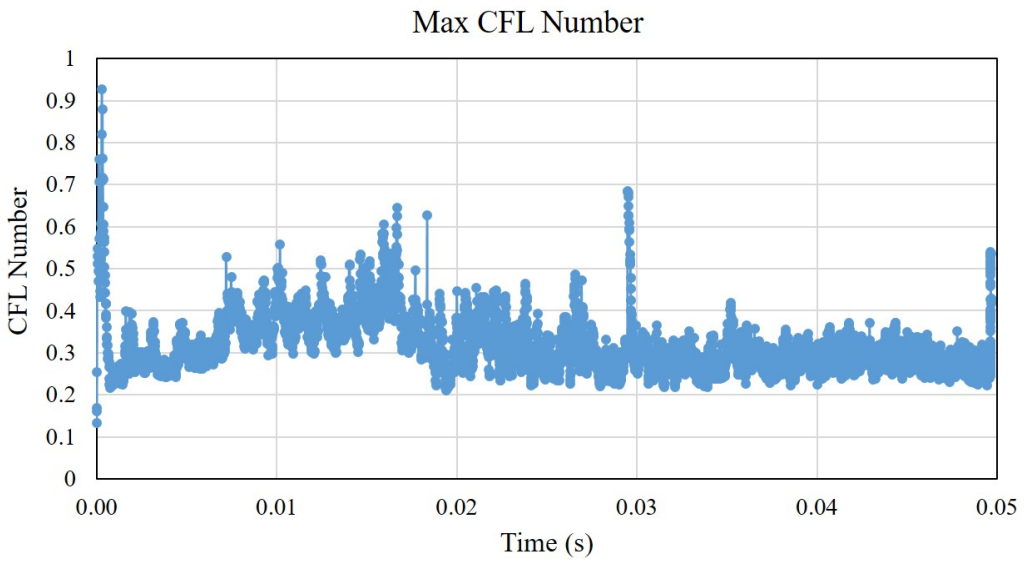

Figure 25: Maximum CFL number in fluid domain

The residual-iteration graph is shown below;

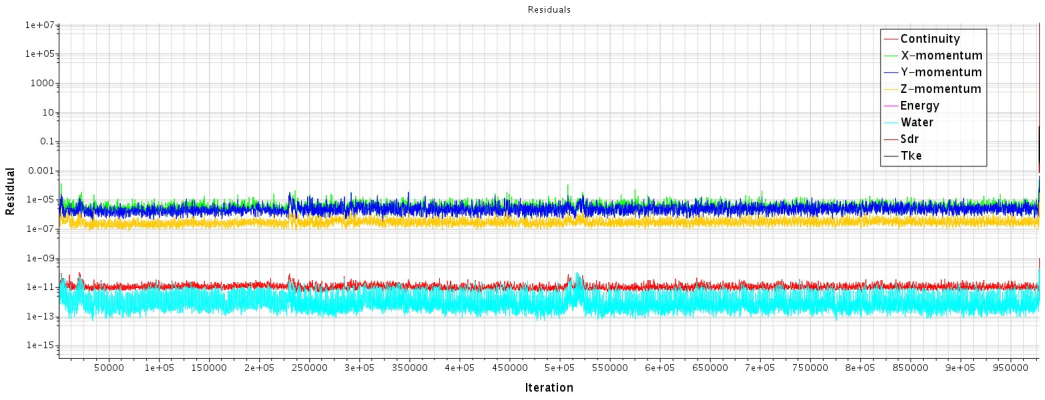

Figure 26: Residual-Iteration graph for 3D simulation by using overset mesh method

4.2 Theoretical Calculations

Theoretical calculations have been done based on leakage equations as tip leakage, face leakage and gearing zone leakage.

Tip leakage has been calculated for all cases which have been performed in 2D

numerical simulations. The results are shown on Table 6. Pressure difference influences the tip leakage significantly. When pressure difference increases from 2 bar to 5 bar, the amount of leaked fluid rises 2.5 times. Besides, rotational speed does not effect tip leakage not as much as pressure difference. Tip leakage reduces very few as gears rotate faster.

Table 7: Theoretical Tip Leakage Calculations for all cases

$Rotational\ Speed(rad/s)$	$Q_{t,2bar}\ (kg/s)$	$Q_{t,5bar}\ (kg/s)$	$Q_{t,8bar}\ (kg/s)$	$Q_{t,10bar}\ (kg/s)$
41.89	0.00211	0.00537	0.00862	0.01079
62.83	0.00208	0.00534	0.00859	0.01076
83.78	0.00205	0.00531	0.00856	0.01073
104.72	0.00202	0.00528	0.00853	0.01070
125.66	0.00199	0.00525	0.00851	0.010368
146.61	0.00196	0.00522	0.0848	0.01065
167.55	0.00193	0.00519	0.00845	0.01062

2D numerical simulations have been done to calculate and investigate only tip leakages. Because, face leakage and gearing zone leakage have been calculated based on the cases which were performed as 3D numerical simulations by using moving reference frame (5 bar-1400 rpm and 10 bar-800 rpm).

For 10 bar 800 rpm case, face leakage at first region (Eqn.28) and second region (Eqn.29) has been calculated 0.00244 kg/s and 0.00257 kg/s . The total amount of leaked fluid from space between faces is approximately 0.005 kg/s. For two gears, net face leakage is 0.01 kg/s. Gearing zone leakage has been calculated 0.00267 kg/s based on Eqn. 30.

For 5 bar 1400 rpm case, face leakage at first region (Eqn.28) and second region

(Eqn.29) has been calculated 0.00113 kg/s and 0.00137 kg/s . The total amount of leaked fluid from space between faces is 0.0025 kg/s. For two gears, net face leakage is 0.005 kg/s. The amount of leaked fluid at gearing zone is 0.00155 kg/s based on Eqn. 30.

4.3 2D Numerical Simulations

The velocity vector scenes of fluid domain for 2, 5, 8, 10 bar at 800 rpm are shown on Figure 27. As is seen from figure, vorticities has been occured in volume packages due to the fact that the volume package which is coming from back tries to push back the leaked fluid from the space between tooth tip and wall. A vorticity has been occured near the wall when pressure difference was 2 bar (Figure 27(a)). At higher pressures, the second one has been occured and became apparent by increasing pressure (Figure 27 (b-d)).

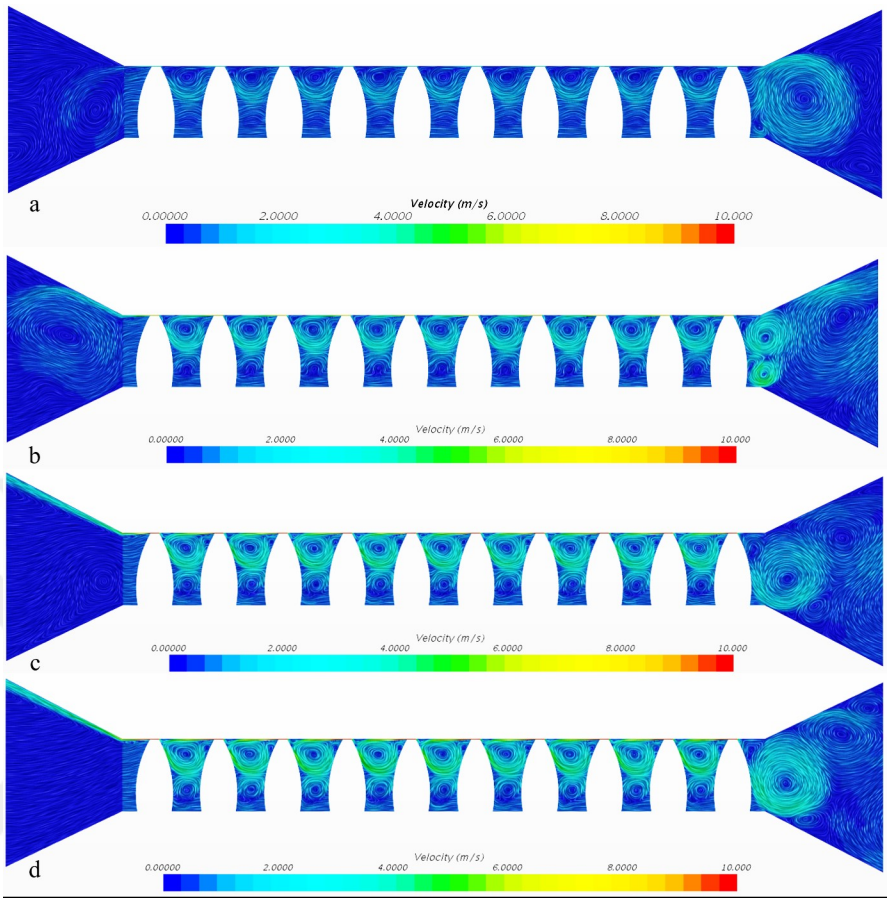

Figure 27: Velocity vector scene for 800 rpm a)2 bar b)5 bar c)8 bar d)10 bar

Pressure distribution at 5 bar and 1400 rpm is shown on Figure 28. Pressure increases gradually from inlet to outlet as in theory.

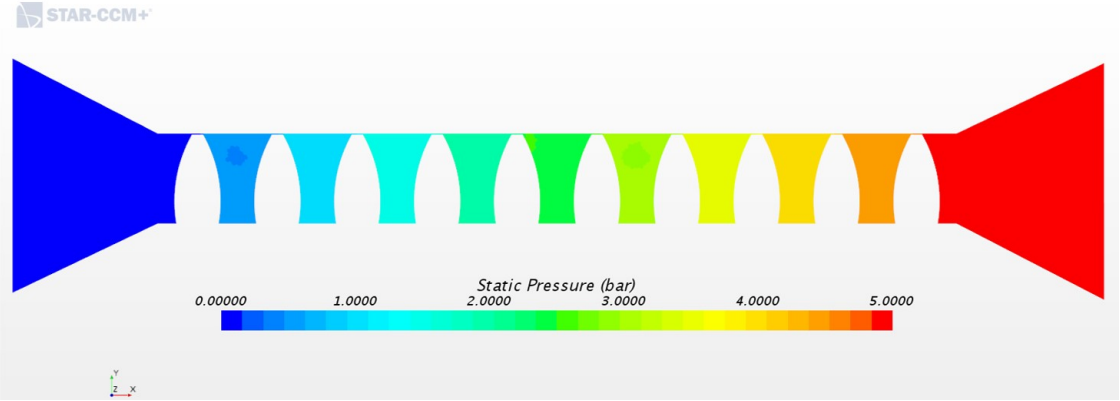

Figure 28: Pressure distribution at ΔP=5 bar and 1400 rpm(2D simulation)

Figure 29 and Figure 30 show the total and static pressure change from input to output in the numerical simulation at 5 bar 1400 rpm. Differences in total pressure indicate viscous losses. Considering that the leakage flow is in the opposite direction to the movement direction of the tooth, it was observed that there was a viscous loss on the right side of the gear (leakage flow inlet) of 0.02 bar on the right side and 0.23 bar on the left side. A loss of only 0.21 bar occurred between the tooth top and the body. A static pressure drop of 0.29 bar at the right side of the tooth in Figure 29 is the result of the conversion of 0.02 bar of viscous loss and a dynamic pressure of 0.27 bar acceleration. On the left side of the tooth, no change in the static pressure also indicates that the dynamic pressure of the liquid coming out of the tooth tip of 0.23 bar in total pressure is completely converted into viscous loss. The difference between the total pressure difference of 0.21 bar and the static pressure difference between 0.22 bar and the difference between the body and the tip is due to the dynamic pressure change caused by acceleration. As a result, the pressure difference at the 5th tooth top is 0.21 bar. However, a pressure differential of 5 bar is theoretically used for design in Couette equations with a difference of 0.5 bar on each tooth top and evenly. That is to say, there is a loss of pressure between the two tines, which is not considered in theory in the leakage outlet and inlet region of the gear.

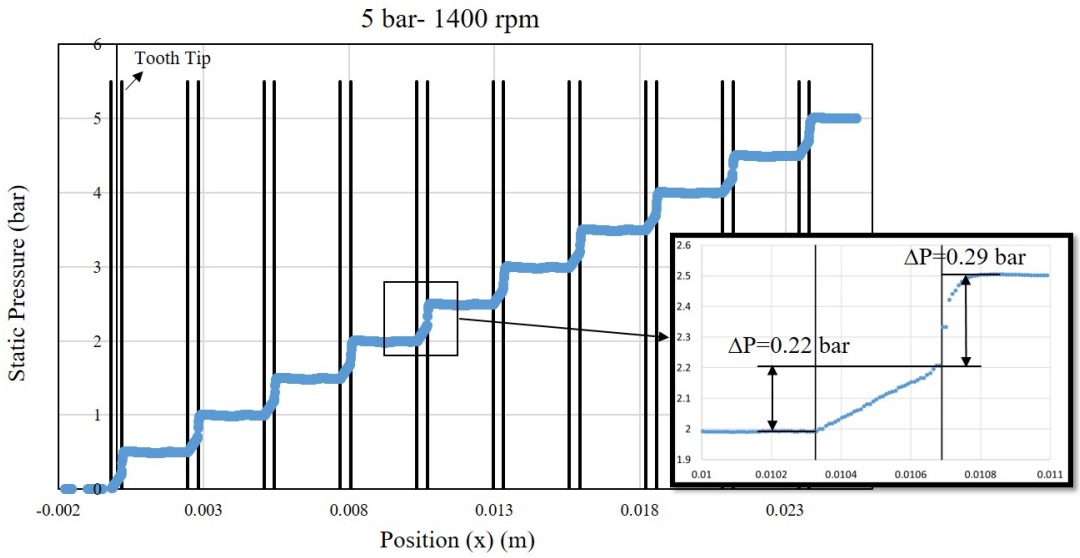

Figure 29: Static pressure- position(x) graph for ΔP=5 bar and 1400 rpm

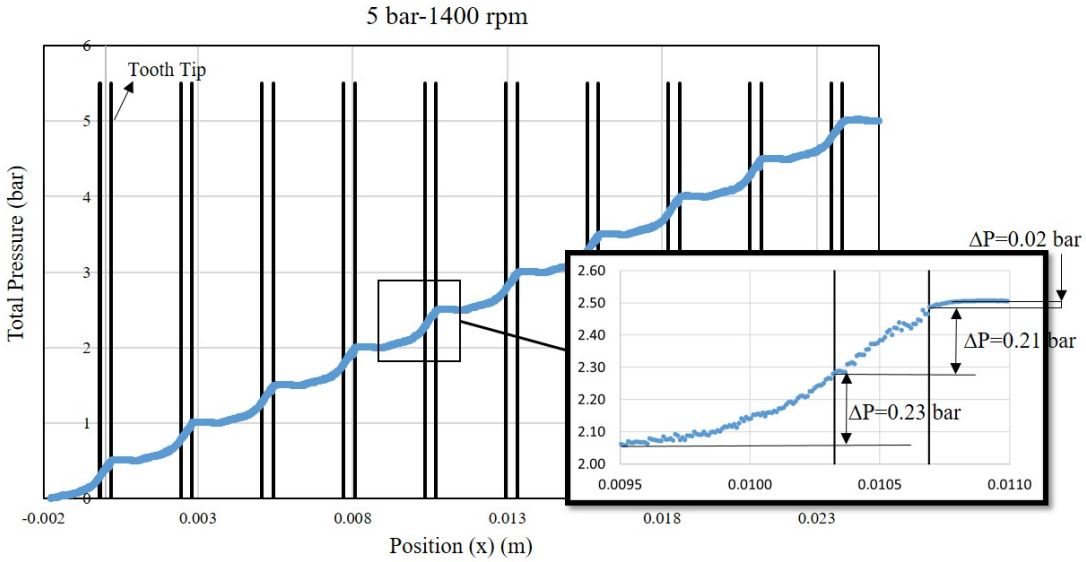

Figure 30: Total pressure- position(x) graph for ΔP=5 bar and 1400 rpm

Dissipation between tooth tip-wall has been observed to investigate the pressure

drop at these points in detail. The term of dissipation in the conservation of mechanical energy that applies to incompressible flow is expressed as follows;

$$\phi = \frac{2\mu}{\rho}\left[\left(\frac{\partial u}{\partial x}\right)^2 + \left(\frac{\partial v}{\partial y}\right)^2 + \left(\frac{\partial u}{\partial y} + \frac{\partial v}{\partial x}\right)^2 + \left(\frac{\partial u}{\partial z} + \frac{\partial v}{\partial z}\right)^2\right] (W/kg) \qquad (35)$$

Dissipation at middle tooth tip (5th teeth) and inlet side of leakage at tooth tip are shown on Figure 31. Particularly on the wall side, the dissipation is seen through the middle of the region between the two teeth. This explains the pressure drop between the tooth tips. In the leakage inlet and outlet side of the tooth top (right and left side, respectively), the dissipation has been observed intensively. In Figure 32, a separation was observed in the velocity vectors at the same point of the tooth tip again. This separation effects increasing the dissipation at body wall and squeezing the flow through body side. Furthermore, the static pressure drop is due to the acceleration in this region. On the outlet side of leakage, the kinetic energy of the leakage flow accelerating between the tooth-body is observed. It should be noted at this point that the structures with vorticity shown in Figure 27 are formed by the shear forces and kinetic energy generated by the leakage flow.

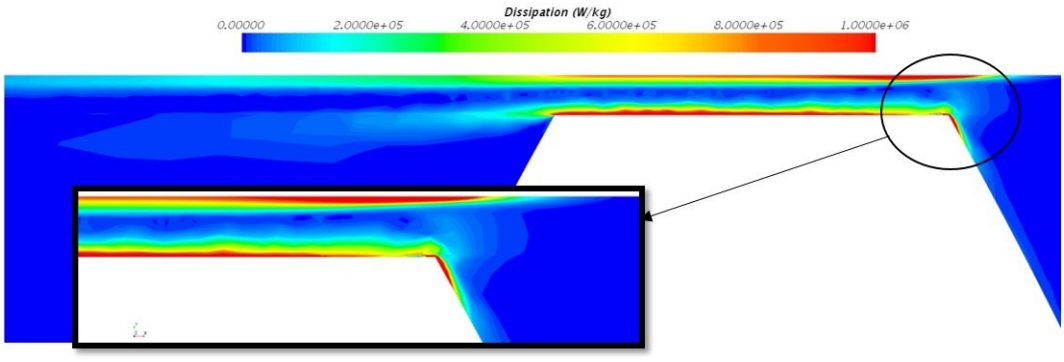

Figure 31: Dissipation scene at middle tooth tip for 5 bar and 1400 rpm (2D simulation)

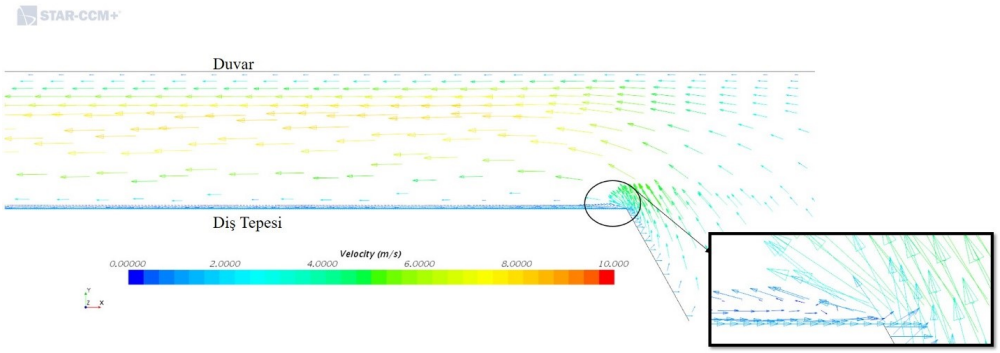

Figure 32: The separation at tooth tip for 5 bar-1400 rpm case (2D simulation)

Tip leakage calculations have been done by using velocity vectors between tooth tip and wall in 2D numerical simulations. Firstly, velocity (i)- centroid (Y) chart has been created to observe velocity data on each center of mesh cells on Star-CCM+ . Then, the data has been exported for each tooth and the formula of finding surface are with integral has been used. The value has been multiplied with density, thickness of pump and number of gear, then the tip leakage at these conditions has been obtained. Based on this calculation, tip leakage values for all cases can be seen on Table 7.

Table 8: 2D Numerical Tip Leakage Calculations for all cases

Rotational Speed(rad/s)	$Q_{t,2bar}$ (kg/s)	$Q_{t,5bar}$ (kg/s)	$Q_{t,8bar}$ (kg/s)	$Q_{t,10bar}$ (kg/s)
41.89	0.00097	0.00184	0.00253	0.00295
62.83	0.00094	0.00182	0.00251	0.00292
83.78	0.00092	0.00179	0.00248	0.00289
104.72	0.00089	0.00177	0.00245	0.00286
125.66	0.00086	0.00174	0.00242	0.00282
146.61	0.00083	0.00171	0.00239	0.00279
167.55	0.00082	0.00169	0.00235	0.00277

The increase in wall temperature due to friction is thought to increase tooth tip leakage. Because the increase in temperature reduces the dynamic viscosity of the liquid. Therefore, numerical simulations have been performed for various wall temperatures at the same pressure and rotational speed (5 bar and 1600 rpm) in order to observe the temperature effect in the tip leakage. In particular, the dynamic viscosity between tooth tip and the wall is significantly reduced due to the high wall temperature as shown in Figure 33. In Figure 34, temperature effect on tip leakages is shown. The graph showed that a temperature increase of $10°C$ resulted in an increase of 10% of the leakage, which reduced the flow efficiency by up to 1%.

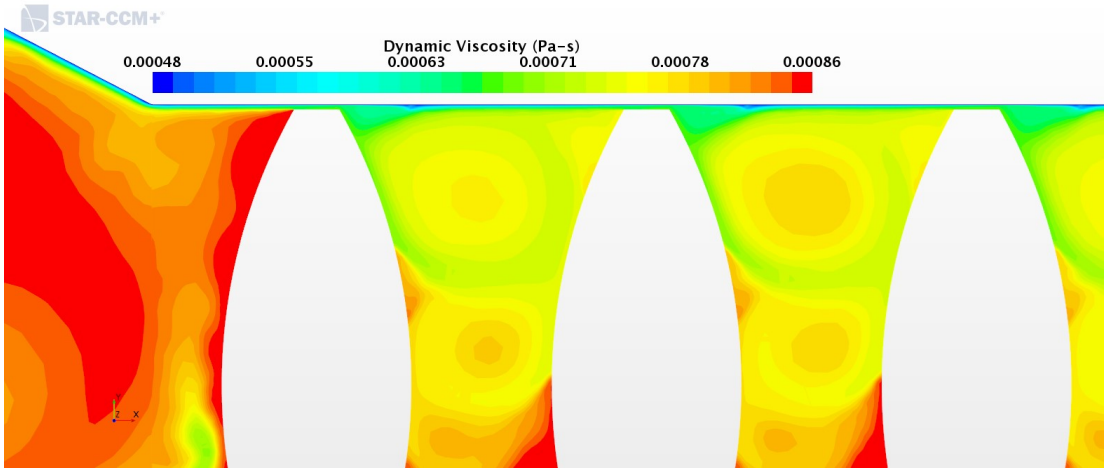

Figure 33: The change of dynamic viscosity in gear pump at T=333 K and 5 bar-1600 rpm

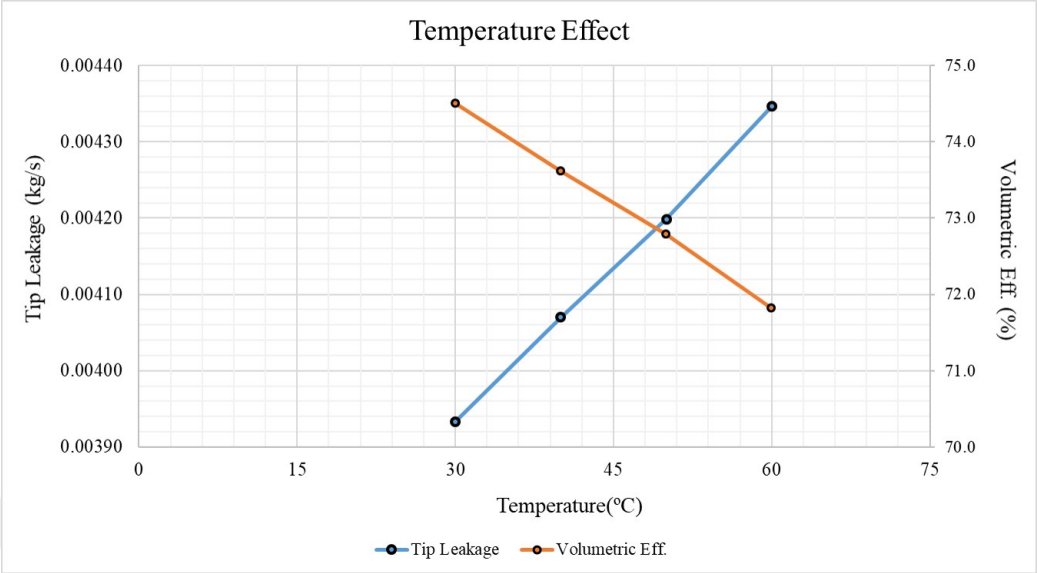

Figure 34: Temperature effect on tip leakages and mass flow rate efficiency for 5 bar-1600 rpm

The residual-iteration graph for 2D numerical simulation in case 5 bar-1400rpm is shown below;

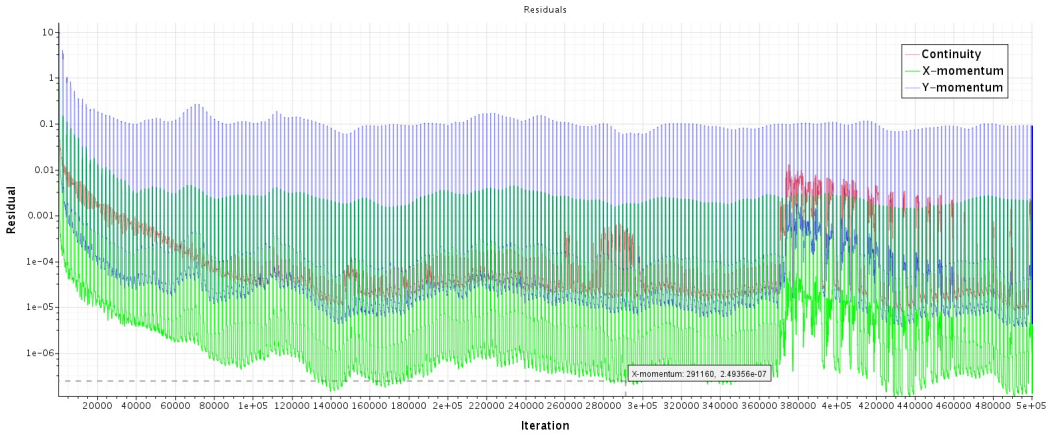

Figure 35: Residual-Iteration graph for 2D numerical simulation in case 5 bar 1400 rpm

4.4 3D Numerical Simulations by using Moving Reference Frame

Vector scenes of the flow inside fluid domain in case 5 bar and 1400 rpm are shown on Figure 36-37-38. The vorticities in volume packages between teeth can be seen on figures as in 2D and other 3D numerical simulations.

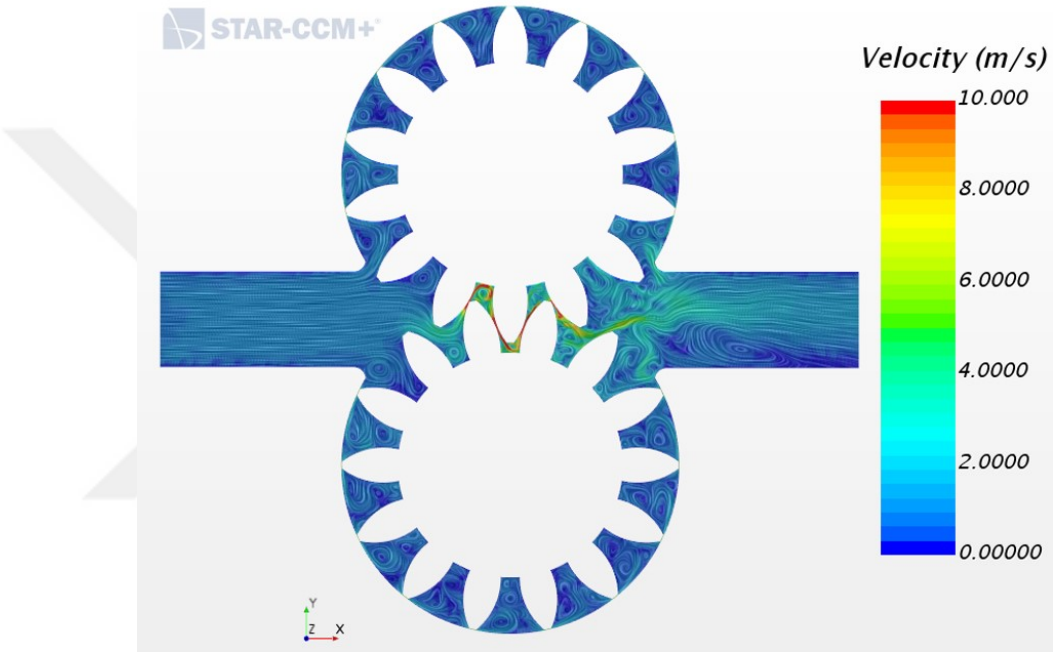

Figure 36: Velocity vector scene of all fluid domain (3D simulation with moving reference frame)

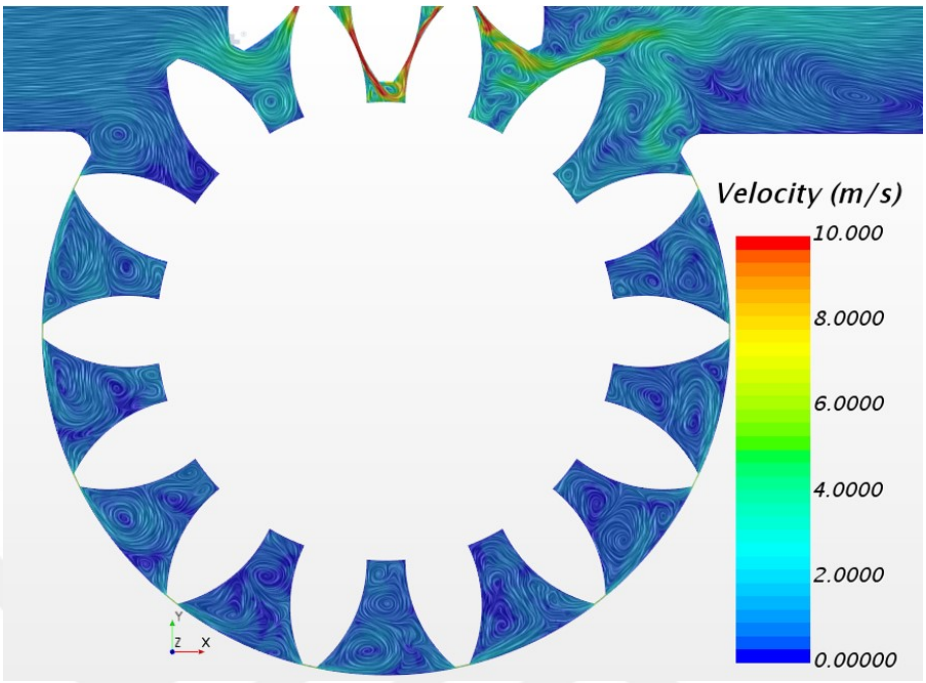

Figure 37: Velocity vector scene of lower gear (3D simulation with moving reference frame)

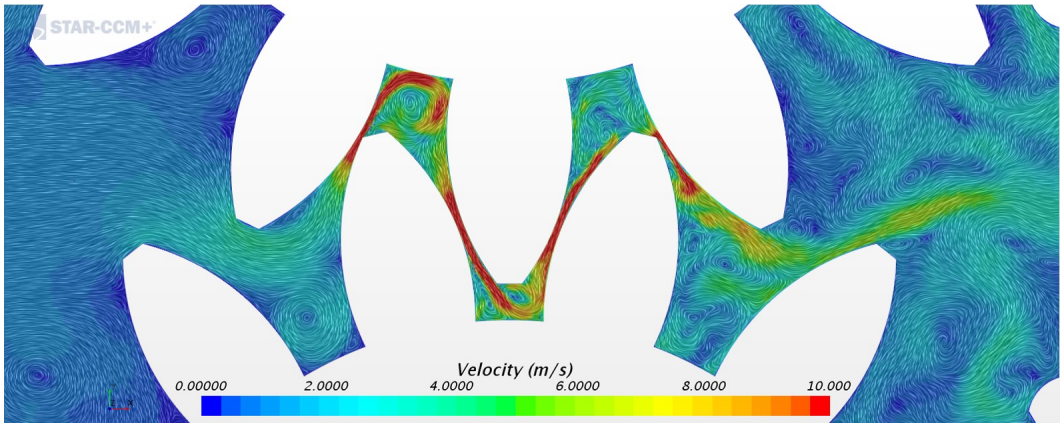

Figure 38: Velocity vectors at gearing zone (3D simulation with moving reference frame)

A plane section has been created on gears faces' to observe the flow and velocity vectors. In Figure 39, velocity vectors at gearing zone show that the flow goes to

body face from gearing zone due to escape from trapped area and pressure difference. Additionally, velocity vectors between tooth tip and wall show that the flow does not go to body face too much as in gearing zone. In Figure 40, vorticities occurred between top and bottom body faces as such in volume packages between tooth.

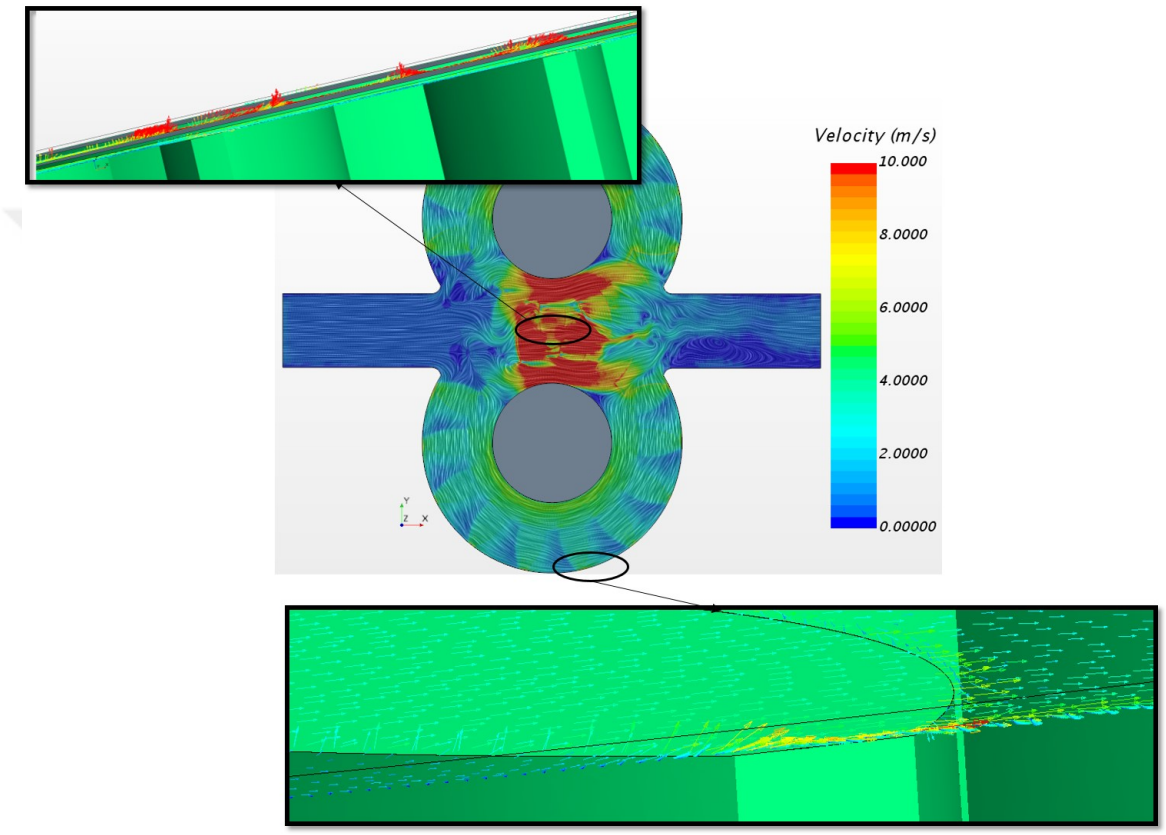

Figure 39: The flow and velocity vectors on gear faces (3D simulation with moving reference frame)

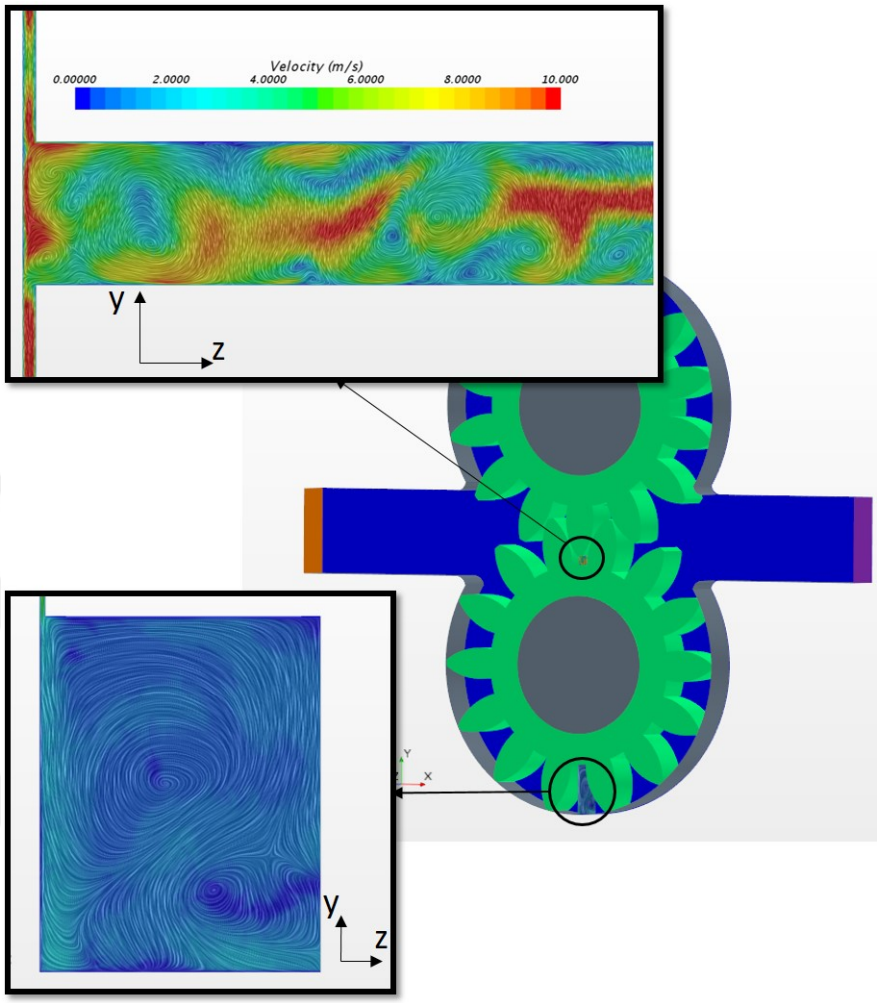

Figure 40: The velocity vectors at z coordinate (3D simulation with moving reference frame)

Pressure distribution in fluid domain are shown on Figure 38. As in theory, pressure increases gradually after each teeth and reaches the given outlet pressure value. Pressure drop can be seen at gearing zone. Pressure reduces approximately to 2 bar from 5 bar.

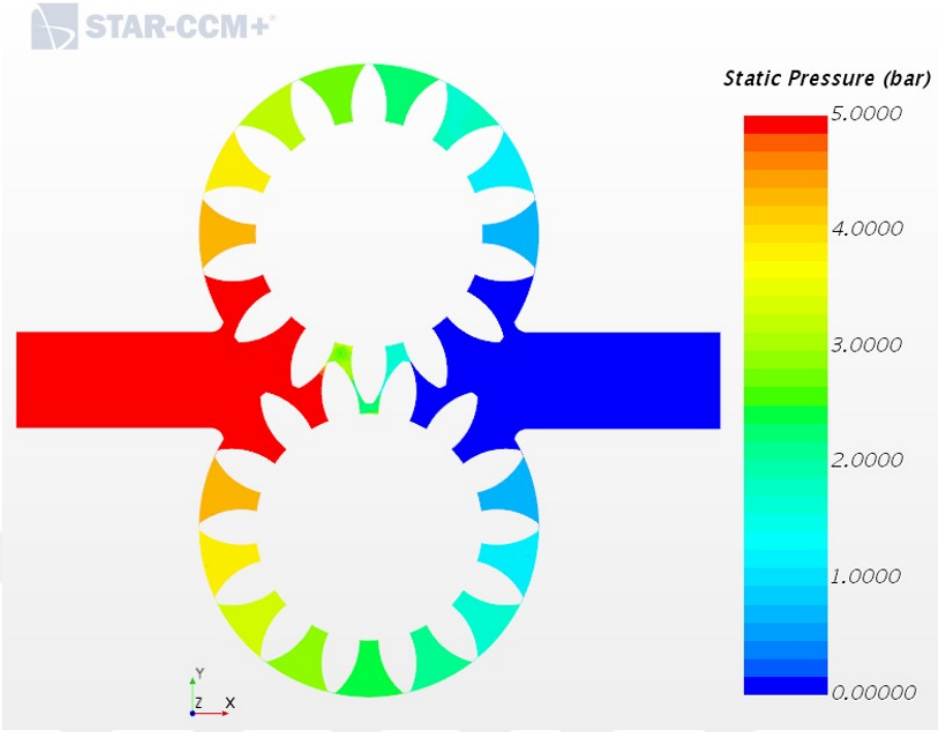

Figure 41: Pressure distribution in fluid domain (3D simulation with moving reference frame)

Figure 42 and Figure 43 show the total and static pressure change from inlet chamber to outlet chamber in the numerical simulation at 5 bar 1400 rpm. As in 2D simulations, viscous losses can be seen on Figure 40. Viscous losses are 0.12 bar at the exit side which is closer side to outlet of tooth (leakage inlet) and 0.33 bar at the other side of tooth (leakage outlet). A loss of only 0.01 bar occurred between the tooth top and the body. On the leakage outlet side of tooth, no change in the static pressure also indicates that the dynamic pressure of the liquid coming out between tooth and the body of 0.33 bar in total pressure is completely converted into viscous loss. The difference between the total pressure difference of 0.01 bar and the static pressure difference between 0.12 bar and the difference between the body and the tip is due to the dynamic pressure change caused by acceleration. As a result, the

pressure difference at the 5th tooth top is 0.01 bar.

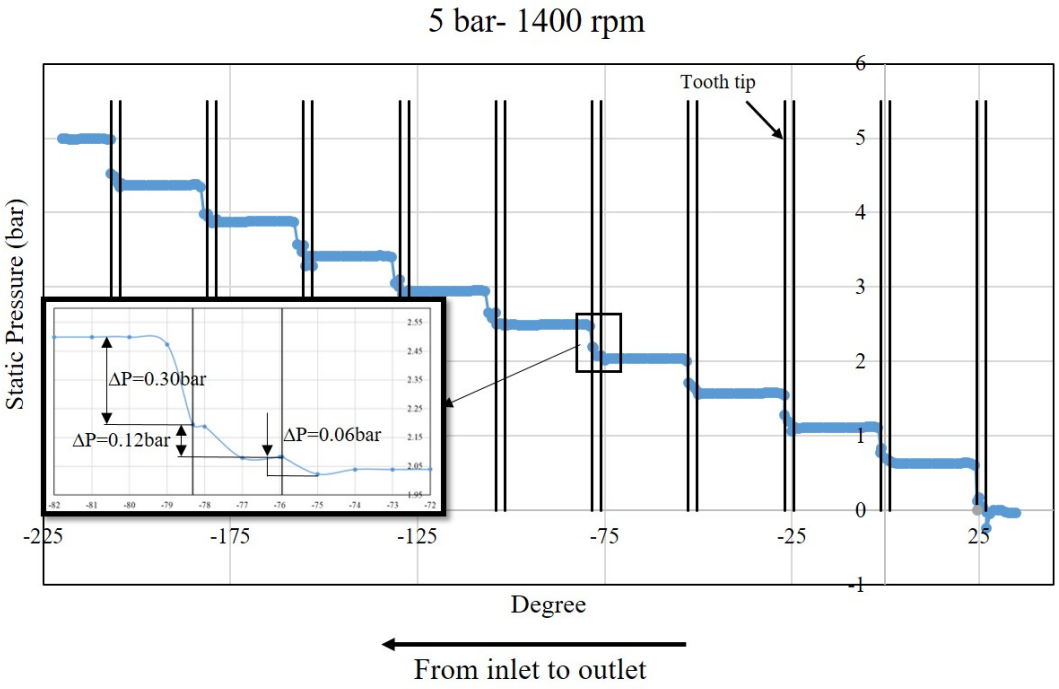

Figure 42: Static Pressure- Degree chart for 5bar-1400 rpm (3D)

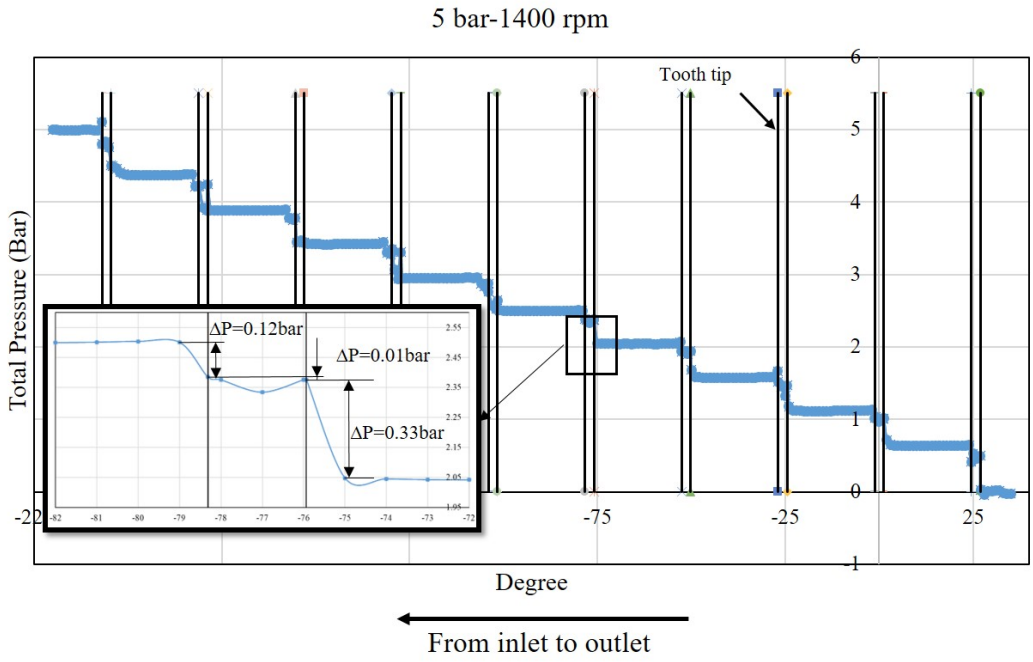

Figure 43: Total Pressure- Degree chart for 5bar-1400 rpm(3D)

As in 2D simulations, dissipation between tooth tip-wall has been observed to investigate the pressure drop at these points in detail. The term of dissipation in 3D is expressed as follows;

$$\phi = \frac{2\mu}{\rho}\left[\left(\frac{\partial u}{\partial x}\right)^2 + \left(\frac{\partial v}{\partial y}\right)^2 + \left(\frac{\partial w}{\partial z}\right)^2 + \left(\frac{\partial u}{\partial y} + \frac{\partial v}{\partial x}\right)^2 + \left(\frac{\partial v}{\partial z} + \frac{\partial w}{\partial y}\right)^2 + \left(\frac{\partial w}{\partial x} + \frac{\partial u}{\partial z}\right)^2 (W/kg) \quad (36)$$

Dissipation at 5th teeth and inlet side of leakage at tooth tip are shown Figure 44. As in 2D numerical simulations, dissipation can be seen at the middle of the region between two teeth, especially at the wall side. This explains pressure drop between tooth tip and wall. In addition, on the outlet side of leakage, the kinetic energy of the leakage flow accelerating between the tooth tip and body is observed. In addition, dissipation at gearing zone are shown on Figure 45. Dissipation can be seen in volume

packages intensely, in particular tooth sides. At the right side of Figure 45, there is more dissipation due to instantaneous pressure drop which arise from trapped fluid between teeth.

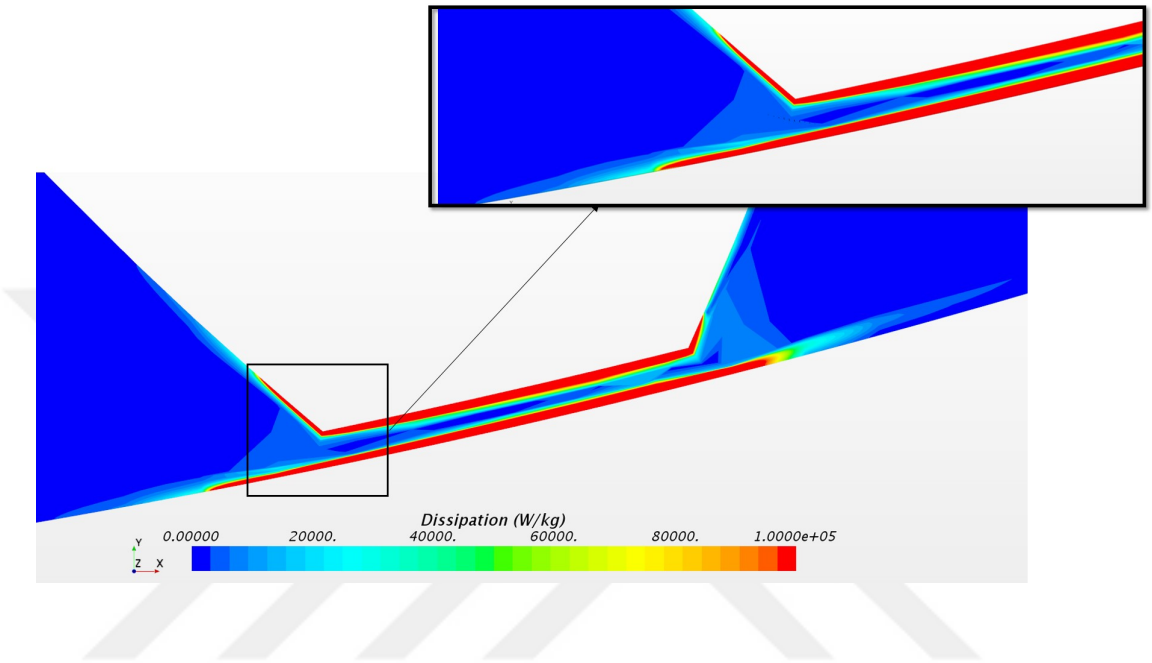

Figure 44: Dissipation scene at middle (5th) tooth in 3D for 5 bar-1400 rpm (3D simulation with moving reference frame)

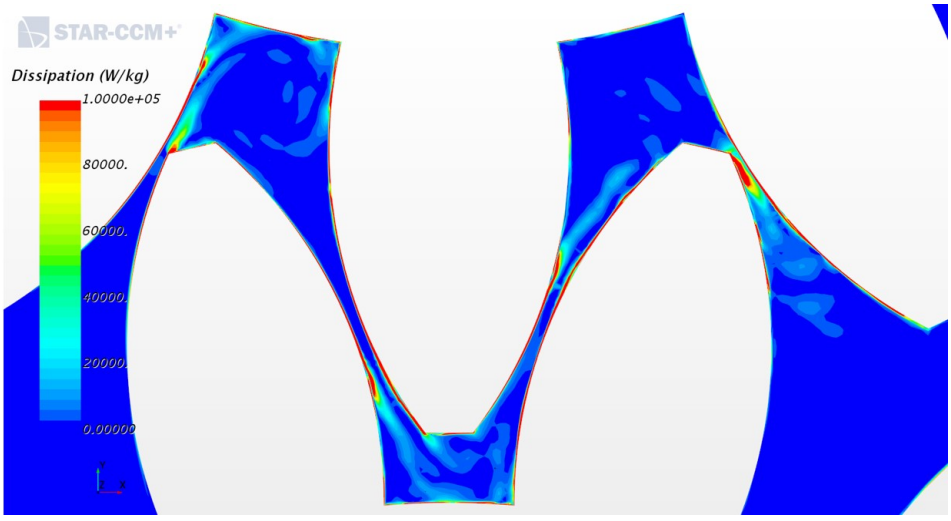

Figure 45: Dissipation scene at gearing zone in 3D for 5 bar-1400 rpm (3D simulation with moving reference frame)

In 3D simulations, all type leakages have been calculated and shown on Table 8. Tip leakages and gearing zone leakages has been calculated as in 2D numerical simulations. For gearing zone calculations, a grid which has a lot of probes at y and z coordinates, called presentation grid, has been created at the location where fluid exits from gearing zone (Figure 46). The velocity(i) values has been exported at each y and z coordinates where presentation grid includes . In excelsheet, the leakage value at gearing zone has been calculated by using surface integral of vector fields. Total leakage value has been obtained from a mass flow report, which is created on Star-CCM+, for backflow to inlet. Face leakage has been calculated by tip leakage and gearing zone leakage subtracting from total leakage.

Table 9: 3D Numerical Leakage Calculations

Leakage Types	$5bar - 1400rpm$	$10bar800rpm$
Tip Leakage(kg/s)	0.00236	0.00336
Face Leakage(kg/s)	0.00874	0.01726
Gearing zone (kg/s)	0.00970	0.01218
Total Leakage(kg/s)	0.0208	0.03280

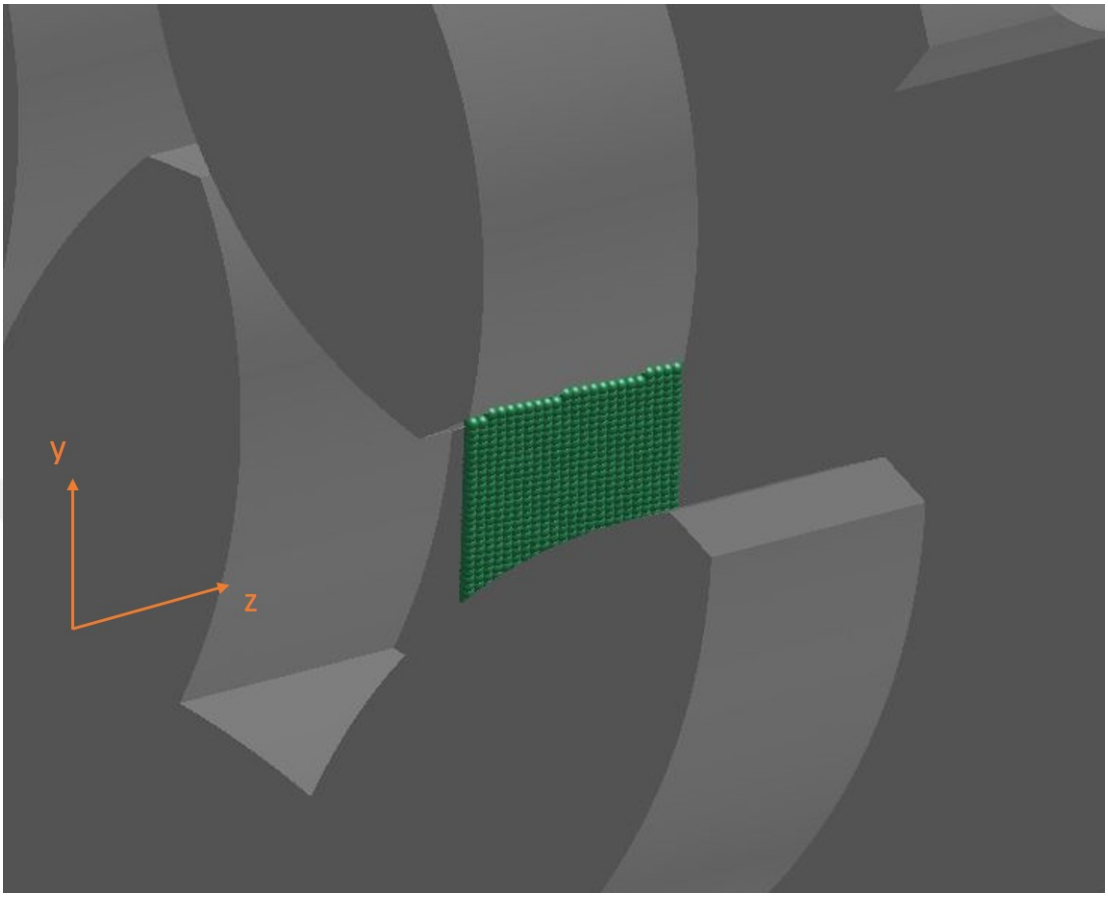

Figure 46: Presentation grid which is created at gearing zone in 3D simulation

The residual-iteration graph for 3D numerical simulation by using moving reference frame method in case 5 bar-1400rpm is shown below;

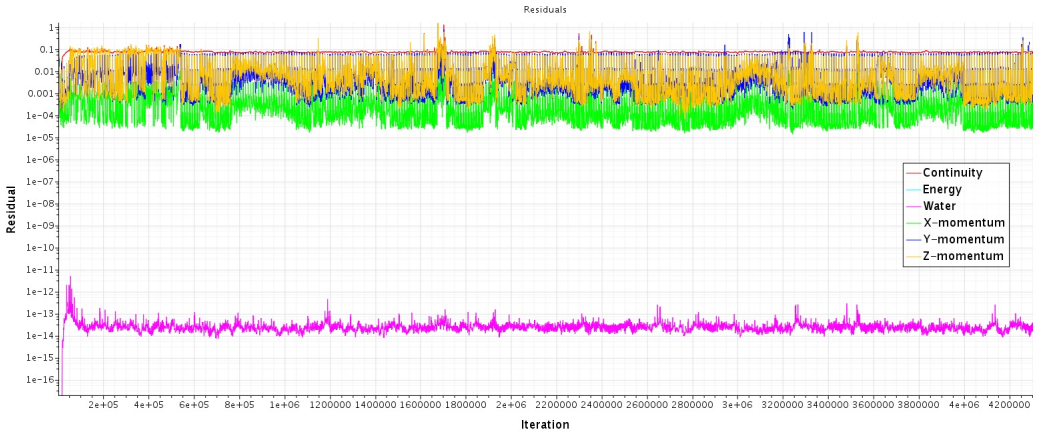

Figure 47: Residual-Iteration graph for 2D numerical simulation in case 5 bar 1400 rpm

4.5 Comparison of Theoretical and Numerical Results

Firstly, velocity vector scenes in 2D and 3D numerical simulations shows that the developed new method in 2D gives accurate results for velocity vectors and vorticities in volume packages (Figure 25, Figure 34).

Theoretical tip leakages are compared with numerical tip leakage calculations on Figure 48. It has been observed that tip leakage does not change much with different rotational speeds, but are markedly increased by pressure difference. In fact, when the rotational speed increases, tip leakage is reduced. However, this reduction in all rotational speeds was found to be about 4%. As seen in Figure 48, there is a deviation between theoretical calculations and numerical simulations. The theoretical calculations in the 2 bars are twice as much as the numerical simulations, and this difference increased as the pressure increased. In numerical simulations, if the pressure increases from 2 bar to 10 bar, the leakage flow is increased three times. But in theoretical calculations the leakage flow rate has increased five times. Mass flow rate efficiency is also shown on Figure 49. Theoretical values are shown with dashed lines, numerical values are shown with solid lines. As pressure increases, mass flow rate

efficiency decreases due to increase of tip leakage. Figure 49 shows that theoretical equations calculate leakage too much.

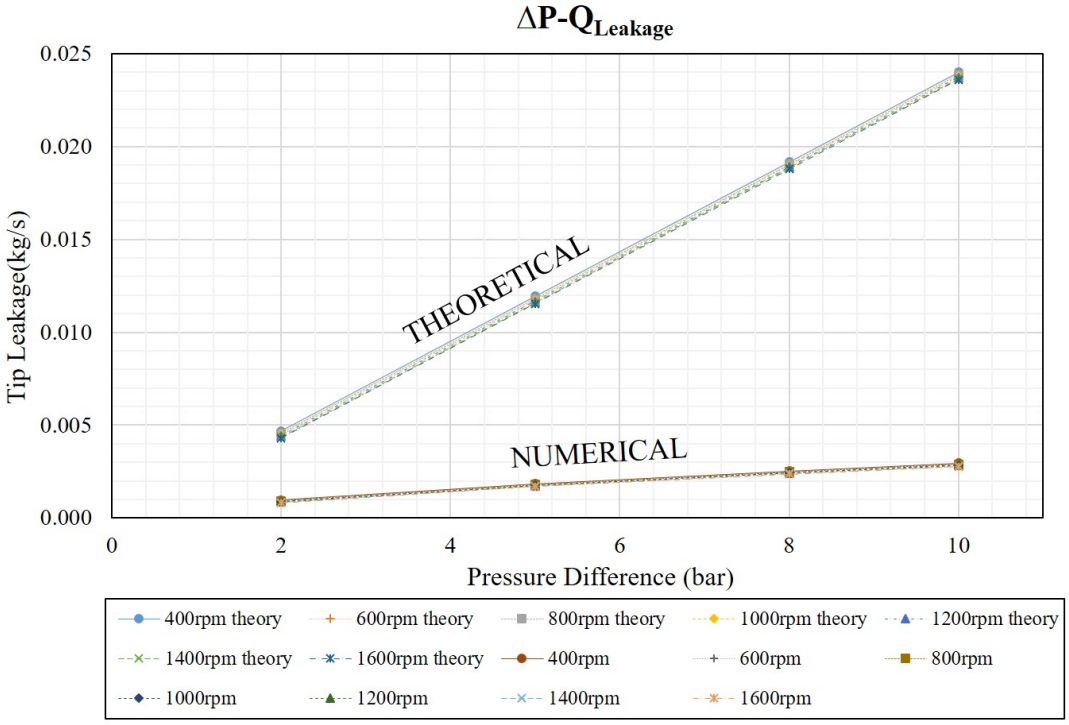

Figure 48: Comparison of 2D numerical simulations and theoretical calculations for the tip leakage

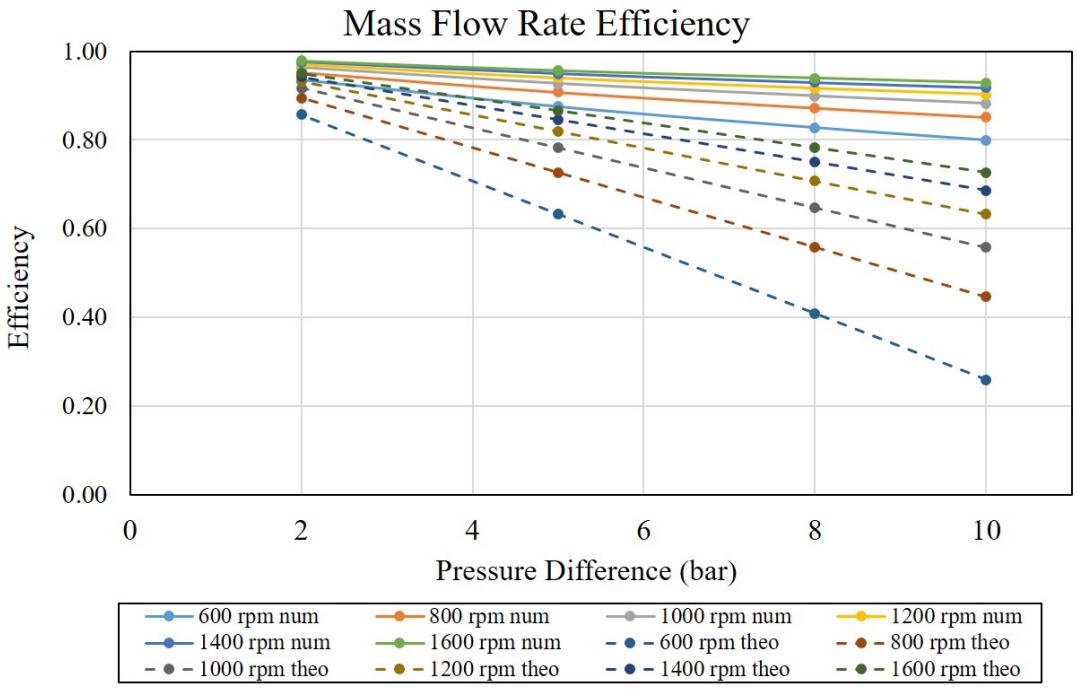

Figure 49: Comparison of 2D numerical simulations and theoretical calculations for the tip leakage

The theoretical calculations of tip leaks have been done based on the fully developed Couette flow assumption. In order to see if there is fully developed flow, 19 plane sections are formed in the middle tooth of this gear, as shown in Figure 49. Velocity profiles have been created for each section and compared with the theoretical velocity profile, which was calculated using the fully developed Couette flow equations.

$$U(y) = \frac{1}{2\eta}\frac{\partial P}{\partial x}\left(y^2 - hy\right) + \frac{y}{h}U_{tip}\,(m/s) \tag{37}$$

For the theoretical velocity profile calculation in Figure 49, $\frac{\partial P}{\partial x}$ is calculated by dividing a pressure differential of 0.5 bar, which must be equal in each tooth top, to the top land (L), which must be equal to a pressure of 5 bar. The tip leakage flow rate (Q) is formed by integrating this velocity profile in the y-direction. None of the velocity profiles in the five planes shown in Figure 45 match the fully developed

flow. There is even a significant asymmetry on the high-pressure side velocity profiles (17 and 18). This asymmetry is the result of the high pressure side flow having a vortex structure before entering the space between tooth tip-body that occur when entering this cavity. That is, the flow, at the beginning of the space, is not exactly parallel to the wall, as assumed in the Couette flow theory. These results show that the assumption is not correct and the profile calculated by Coutte flow equations does not reflect the truth.

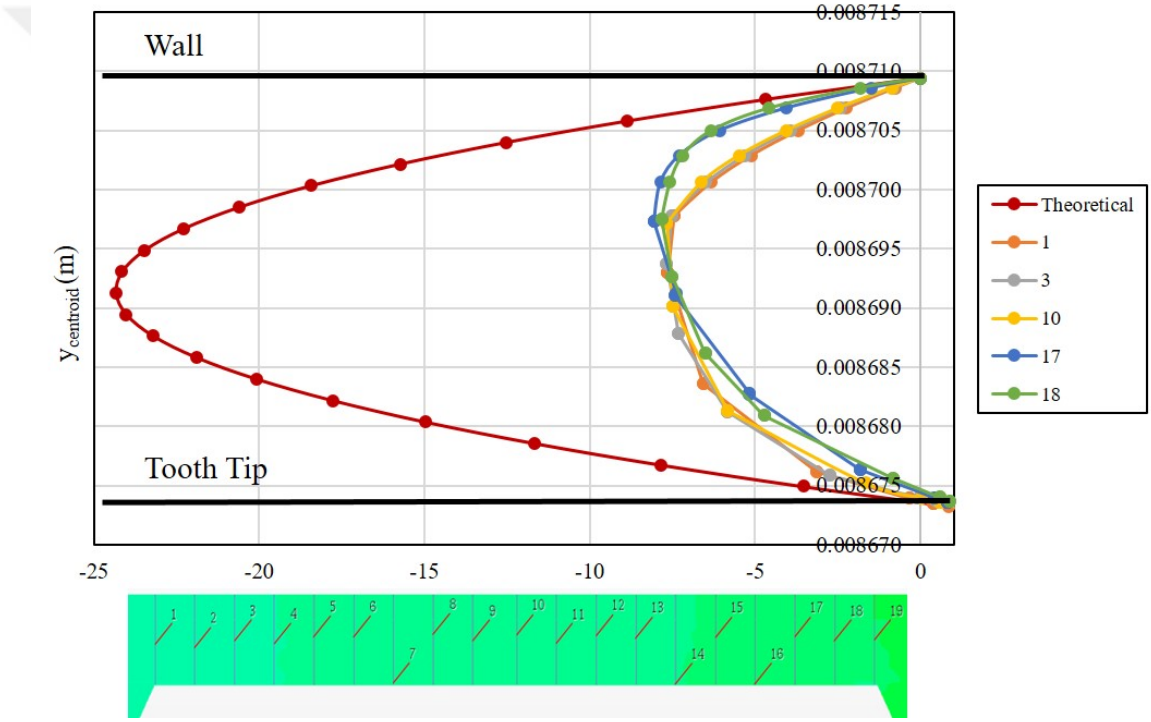

Figure 50: Comparison of velocity profile of theoretical and some plane sections in 2D between gear tip and wall for 5 bar, 1400 rpm case

In 3D numerical simulations, 14 line probes has been created instead plane sections at the middle tooth to see that there is fully developed flow or not. The same results has been observed as in 2D numerical simulations (Figure 50). Especially for 2, there is a significant asymmetry on the high pressure side velocity profiles.

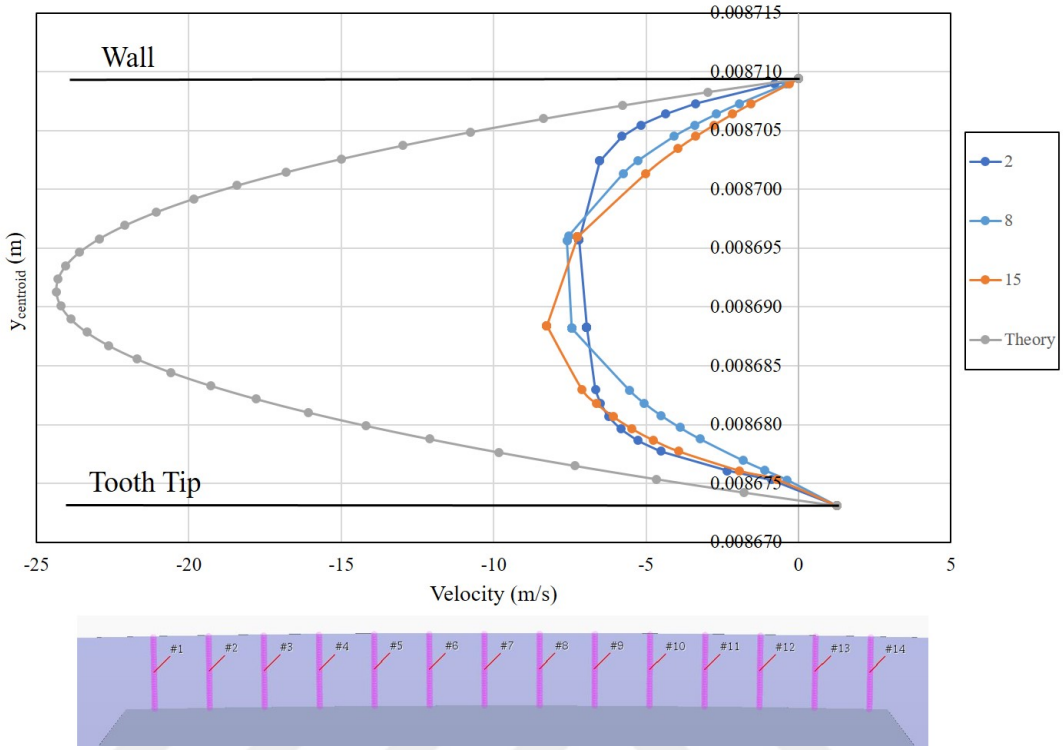

Figure 51: Comparison of velocity profile of theoretical and some line probes in 3D between gear tip and wall for 5 bar, 1400 rpm case

In Figure 51, the theoretical calculations can be made by means of the difference in pressure on the tooth top in 2D numerical simulations; a new velocity profile has been obtained. The maximum speed has decreased from 25 m / s to 10 m / s. Although the difference between the theoretical fully developed Couette flow calculation and the numerical calculations is reduced, the fully developed flow assumption is not fully valid. The main source of this discrepancy is the irregularity in the right (leakage) of the gear and the viscous losses it creates.

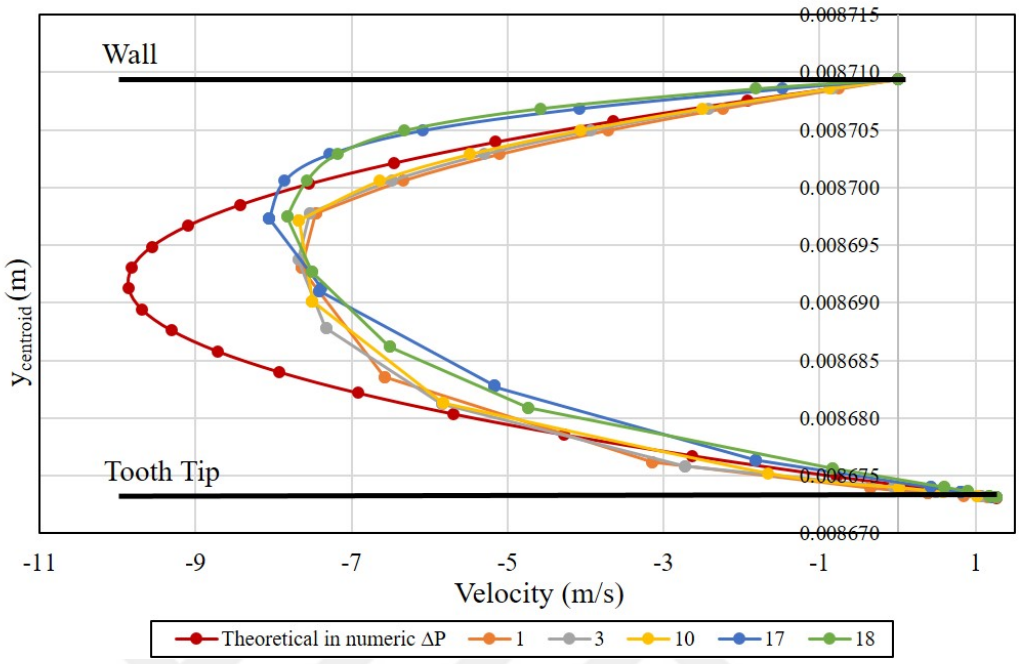

Figure 52: Comparison of velocity profile of numerical ΔP value in theory and some plane sections in 2D between gear tip and wall

The theoretical calculations can be made by means of the difference in pressure on the tooth top in 3D numerical simulations (Figure 52).The maximum velocity decreases to 5 m/s approximately and this value is less than numerical values. Because, total pressure drops dramatically at 5th teeth in this case due to viscouss losses.

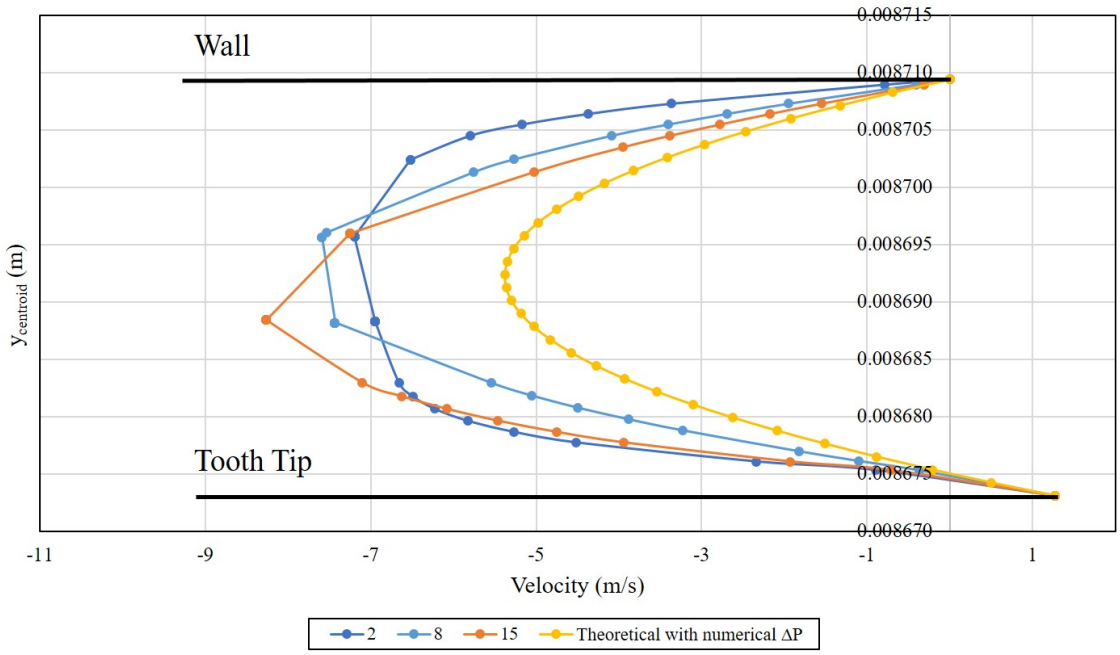

Figure 53: Comparison of velocity profile of numerical ΔP value in theory and some line probes in 3D between gear tip and wall

Comparison of theoretical and numerical calculations based on leakages in case 5 bar-1400 rpm are shown on Table 9. Tip leakage has similar values for 2D and 3D numerical simulations. The difference in tip leakages between 2D and 3D numerical results can arise from z coordinate in 3D simulations. Theoretical tip leakage is twice as high than numerical tip leakages. Theoretical value in 2D numerical ΔP is closer to 2D numerical value. But, theoretical tip leakage in 3D numerical ΔP is less than all tip leakage values due to more pressure drop between tooth tip and wall than 2D numerical simulation. In addition, there is a deviation for face leakage and gearing zone leakage between theoretical calculations and 3D numerical simulations. Especially, gearing zone causes a big difference in total leakage between theoretical and 3D numerical calculations. The numerical calculation method or ignorance of z coordinate in theoretical equation can cause this deviation between numerical and theoretical results at gearing zone.

Table 10: Comparison of Theoretical and Numerical Calculations based on Leakages for 5 bar-1400 rpm

Leakage Types	*Theoretical*	*Numerical* (2*D*)	*Numerical* (3*D*)	*Theoretical calculated by using Numerical dP from 2D sim.*	*Theoretical calculated by using Numerical dP from 3D sim.*
Tip Leakage (kg/s)	0.0052	0.0018	0.0024	0.0021	0.0011
Face Leakage (kg/s)	0.0050	-	0.0158	-	-
Gearing zone (kg/s)	0.0015	-	0.0027	-	-
Total Leakage (kg/s)	0.0118	-	0.0208	-	-

Table 11: Comparison of Theoretical and Numerical Calculations based on Leakages for 10 bar-800 rpm

Leakage Types	*Theoretical*	*Numerical* (2*D*)	*Numerical* (3*D*)	*Theoretical calculated by using Numerical dP from 2D sim.*	*Theoretical calculated by using Numerical dP from 3D sim.*
Tip Leakage (kg/s)	0.0107	0.0030	0.0034	0.0058	0.0075
Face Leakage (kg/s)	0.0100	-	0.0256	-	-
Gearing zone (kg/s)	0.0027	-	0.0038	-	-
Total Leakage (kg/s)	0.0234	-	0.0328	-	-

In table 10, 2D and 3D numerical simulations and theoretical calculations are compared in case 10 bar and 800 rpm. Theoretical tip leakage calculation is three times higher than numerical simulations' results at this time. It shows that the difference between results for tip leakage increases, as pressure difference rises. 2D and 3D numerical values are closer than the other case. Besides, theoretical value in 2D numerical ΔP is not close to 2D numerical value for this case. In particular, the difference between 3D numerical value and theoretical value in 3D numerical ΔP get higher than the results in 2D ones. Furthermore, the deviation seems between theoretical and 3D numerical results for gearing zone leakage, similarly with the other

case.

CHAPTER V

CONCLUSION

In this thesis, leakages has been investigated by comparison of theoretical calculations and numerical simulations. Due to the complex geometry of the external gear pumps, the 2D numerical simulations have been performed by a developed new method. In this method, the geometry is simplified to the area where only tip leakage could be observed. By flattening the flow area between the gear and body having a circular inclination, the rotational speeds have been converted to linear velocity and the flow has been evaluated as in the Couette flow equations used in the same design theory. The reservoirs next to the gears represent the inlet and outlet ponds where the volume packs are received and transported. Additionally, 3D numerical simulations have been done with two different methods as overset "chimera" mesh method and moving reference frame method. Because of long computational time, 3D simulations with using moving reference frame method have been performed only for 2 cases instead of all cases.

3D numerical simulation by using overset mesh method could not been finalized due to long comuputational time and not obtaining accurate and reliable results such as problem for pressure distribution in fluid domain and how "contact zone" method effect the flow at gearing zone. This simulation needs improving and optimizing the mesh for reliable results and reduce the computational time.

Numerical simulations have been compared with the theoretical calculations, and the theoretical calculations with simplified Couette flow equations have been analyzed and these equations needs to improve and optimize based on pressure drop.

For tip leakage, there is a deviation between theoretical and 2D-3D numerical

results. Firstly, energy dissipation at tooth tip causes pressure drop at this location. When the pressure difference is 5 bar, pressure should increase by 0.5 bar after each tooth in theory; the average increased by 0.21 bar in 2D simulations. This value is less in 3D simulation as 0.12 bar. Pressure drop between tooth tip and wall causes a more deviation between theoretical and numerical calculations. These results show that theoretical leakage equations overestimate tip leakage too much. In other words, film thickness of gear pump can be designed smaller than it should be. However, this causes production problems.

For face and gearing zone leakage, there is a deviation between theoretical calculations and 3D numerical simulations. Especially, the difference of gearing zone leakage has been investigated. Face leakage can be calculated firstly and then gearing zone is calculated by tip and face leakage subtracting from total leakage.

The effect of the heat passing from the heated body to the liquid is also shown. The dynamic viscosity decreases as the wall temperature increases due to friction between the tooth tip and the wall. This means that the liquid delivered to the outlet with viscosity decreases; thus increasing tooth tip leakage. In every 10C increase in wall, tip leakage is increased by 10% while flow efficiency decreases by 1%.

Consequently, theoretical leakage calculations are not reliable and usable for gear pump design. Theoretical equations should be improved and formed with considering dissipation.

As future work, a reliable method should be improved to calculate gearing zone and face leakages. In addition, for tip leakage, theoretical equations should be improved and formed new equation with considering viscous losses between tooth tip and wall. Temperature change on case wall will be observed on 2D and 3D numerical simulations in detail.

Bibliography

[1] E. Koç and F. Canbulut, "Pozitif Deplasmanl Pompa ve Motorlarda ç Akkan Kaça," 1985.

[2] I. J. Karassik, J. P. Messina, P. Cooper, and C. C. Heald, *Pump Handbook*. 2001.

[3] G. Ghionea, C. Ioan, and P. Tiriplic, "Simulation of the Working Conditions for a Gear Pump Using Finite Element Analysis Method," vol. 2012, no. Xxvi, pp. 21–28, 2012.

[4] A. A. Yusof, F. Wasbari, M. S. Zakaria, and M. Q. Ibrahim, "Slip flow coefficient analysis in water hydraulics gear pump for environmental friendly application," *IOP Conference Series: Materials Science and Engineering*, vol. 50, p. 012016, dec 2013.

[5] J. Schiffer, H. Benigni, and H. Jaberg, "Development of a novel miniature high-pressure fuel pump with a low specific speed," *Proceedings of the Institution of Mechanical Engineers, Part D: Journal of Automobile Engineering*, vol. 227, no. 7, pp. 997–1006, 2013.

[6] R. S. Devendran and A. Vacca, "Optimal design of gear pumps for exhaust gas aftertreatment applications," *Simulation Modelling Practice and Theory*, vol. 38, pp. 1–19, 2013.

[7] J. Ghazanfarian and D. Ghanbari, "Computational Fluid Dynamics Investigation of Turbulent Flow Inside a Rotary Double External Gear Pump," *Journal of Fluids Engineering*, vol. 137, no. 2, p. 021101, 2014.

[8] G. Houzeaux and R. Codina, "A finite element method for the solution of rotary pumps," *Computers & Fluids*, vol. 36, no. 4, pp. 667–679, 2007.

[9] R. Castilla, P. J. Gamez-Montero, N. Ertrk, A. Vernet, M. Coussirat, and E. Codina, "Numerical simulation of turbulent flow in the suction chamber of a gearpump using deforming mesh and mesh replacement," *International Journal of Mechanical Sciences*, vol. 52, no. 10, pp. 1334–1342, 2010.

[10] R. Castilla, P. J. Gamez-Montero, D. del Campo, G. Raush, M. Garcia-Vilchez, and E. Codina, "Three-Dimensional Numerical Simulation of an External Gear Pump With Decompression Slot and Meshing Contact Point," *Journal of Fluids Engineering*, vol. 137, no. April, p. 041105, 2015.

[11] W. Strasser, "CFD Investigation of Gear Pump Mixing Using Deforming/Agglomerating Mesh," *Journal of Fluids Engineering*, vol. 129, no. 4, p. 476, 2007.

[12] E. A. Acikgoz, M. Gelisli, "COK KADEMELI POMPA PERFORMANSININ CFD YONTEMIYLE BELIRLENMESI," *Anova Muhendislik Ltd. Sti.*, pp. 1–6.

[13] M. Močilan, Š. Husár, J. Labaj, and M. Žmindák, "Non-stationary CFD Simulation of a Gear Pump," in *Procedia Engineering*, vol. 177, pp. 532–539, 2017.

[14] T. XIAO and H. ANG, "COMBINATION OF MESH DEFORMATION AND OVERSET GRID FOR SIMULATING UNSTEADY FLOW OF INSECT FLIGHT," 2009.

[15] R. Shenoy, M. J. Smith, and M. A. Park, "Unstructured Overset Mesh Adaptation with Turbulence Modeling for Unsteady Aerodynamic Interactions," *Journal of Aircraft*, vol. 51, no. 1, pp. 161–174, 2014.

[16] L. Ferrier, M. Vezza, and H. Zare-Behtash, "Improving the aerodynamic performance of a cycloidal rotor through active compliant morphing," *The Aeronautical Journal*, vol. 121, pp. 901–915, jul 2017.

[17] F. Mechanics, M. Mostly, C. Vol, D. Approach, and C. Volume, "Fluid Mechanics for Mechanical Engineers / Integral Analysis of Fluid Flow,"

[18] V. Krieger, R. Perić, J. Jovanović, H. Lienhart, and A. Delgado, "Toward design of the antiturbulence surface exhibiting maximum drag reduction effect," *Journal of Fluid Mechanics*, vol. 850, pp. 262–303, 2018.

VITA

Deniz İmamoğlu received the B.Sc. degree in Mechanical Engineering Department from Yıldız Technical University, Istanbul, Turkey, 2014. He is currently pursuing the M.Sc. degree in Mechanical Engineering Departmen at Ozyegin Universty under the supervision of Dr-Ing. Özgür Ertunç. His research interests involve turbomachinery and multiphase flows.